Novel segmentation algorithm for high-throughput analysis of spectral domain-optical coherence tomography imaging of teleost retina

by

© Kent Barter

A thesis submitted to the

School of Graduate Studies

in partial fulfillment of the

requirements for the degree of

Master of Science

Supervisor: Dr. Meruvia-Pastor, Dr. Paradis and Dr. Gendron

Department of Computer Science

Memorial University of Newfoundland

April 2023

St. John's   Newfoundland

Abstract

Aim Spectral Domain-Optical Coherence Tomography (SD-OCT) has become an essential tool to assess the health of ocular tissues in live subjects. The processing of SD-OCT images, in particular from non-mammalian species, is a labour-intensive manual process due to the lack of access to analytical programs. The work presented herein describes the development and implementation of a novel computer algorithm for quantitative analysis of SD-OCT images of live teleost eyes. We hypothesized that this algorithm, in comparison to manual segmentation of SD-OCT images, will allow more precise measurement, with significantly higher throughput capacity, of retinal architecture in live teleost ocular tissue.

Methods Automated segmentation processing of SD-OCT images of the retinal layers was developed using a novel algorithm based on thresholding, which operates on the pixel values contained in an image. The algorithm measured the thickness characteristic of the retina present in the input dataset to provide increased accuracy and repeatability of SD-OCT analysis over manual measurements. The program was also designed to allow adjustments of the thresholding variables to suit any specific image set. A heat map software was created alongside the algorithm to plot the SD-OCT image measurements as a colour gradient.

Results Automated segmentation analysis of the retinal layers from SD-OCT images enabled analysis of a large volume of imaging data of teleost ocular structures in a short time. The algorithm was just as accurate when compared to manual measurements and provided repeatability as measurements could be quickly reassessed to confirm previously determined results. This is the case as the algorithm can generate hundreds of retinal thickness measurements per image for a large number of images for a given dataset. This algorithm can be deemed as repeatable as each input will always produce the same output due to the thresholding methods used. This is the case as thresholding is a finite mathematical process to determine a range of values. The measurements produced from this assessment were represented by a heat map software that directly converted the measurements taken from each processed image to represent the changes in thickness across the whole retinal scan.

Conclusions Our work addresses the need for accurate and high-throughput SD-OCT data analysis for the retinal tissues of teleosts where previously no such program existed. Our heat mapping software enables the visualization of the retinal thickness across the whole retinal scans facilitating the comparison of specimens and localization of areas of interest. Our novel algorithm provides the first tools to analyze SD-OCT scans of non-mammalian species at a faster rate than manual analysis, increasing the potential of future research output. The adaptability of our programs makes them potentially suitable for the analysis of SD-OCT scans from other non-mammalian species.

Acknowledgments

We are grateful for the expert help from Danny Boyce and staff at the Joe Brown Aquatic Research Facility of Memorial University. We also thank Dr. William Driedzic of Department of Ocean Sciences, Memorial University, for access to cunners and Dr. J. Vance (The Spective Group, Raleigh-Durham, NC) for zebrafish SD-OCT scan data. We are also Grateful for Dr. Pierre-Paul Bitton for his help in reviewing this thesis.

Publication

Publication: The work presented in this thesis was published in the journal of Molecular Vision, with the authors retaining fully copyright: Barter, Kent R., et al. "Novel segmentation algorithm for high-throughput analysis of spectral domain-optical coherence tomography imaging of teleost retinas." (2022) [1].

Dedication

I here by dedicate this thesis to those that dedicate themselves to the pursuit of excellence in the fields of science and medicine. Their contribution to the world knows no bounds, and with this combined history of gained wisdom, gratitude and persistence that we may strive to create a better tomorrow.

Author's Declaration

This thesis consists of material all of which I authored or co-authored: see Statement of Contributions included in the thesis. This is a true copy of the thesis, including any required final revisions, as accepted by my examiners. I understand that my thesis may be made electronically available to the public.

Statement of Contributions

Conceptualization: Kent Barter[1] and Dr. Oscar Meruvia-Pastor[1]; Design: Kent Barter, Dr. Hélène Paradis[2], Dr. Robert Gendron[2] and Dr. Oscar Meruvia-Pastor[1]; Software: Kent Barter[1]; Investigation: Kent Barter[1], Dr. Hélène Paradis[2], Dr. Robert Gendron[2] and Dr. Josué Lilly[3]; Data analysis: Kent Barter[1], Dr. Hélène Paradis[2] and Dr. Josué Lilly[3]; Writing: Kent Barter[1], Dr. Hélène Paradis[2], Dr. Robert Gendron[2] and Dr. Oscar Meruvia-Pastor[1];

Affiliations

1 - Department of Computer Science, Memorial University, St. John's, A1B 3V6, NL, Canada. 2 - Division of Biomedical Sciences, Faculty of Medicine, Memorial University, St. John's, A1B 3V6, NL, Canada. 3 - Department of Ophthalmology, College of Medicine, University of Saskatchewan, Saskatoon, SK, S7K 0M7, Canada.

The candidate certifies that: The above statement correctly reflects the nature

and extent of the candidate's contributions to this work, and the nature of the contribution of each of the co-authors; and the candidate wrote all or majority of the text.

Funding

Contents

List of Figures

Chapter 1

Introduction

1.1 Overview of the project

Spectral Domain Optical Coherence Tomography (SD-OCT) has become an essential
tool to assess the health of ocular tissues in live subjects. The processing of SD-
OCT images, in particular from non-mammalian species, is a labor-intensive manual
process due to the lack of access to analytical programs. The work presented herein
describes the development and implementation of a novel computer algorithm for
quantitative analysis of SD-OCT images of live teleost eyes. We hypothesized that
the algorithm, in comparison to manual segmentation of SD-OCT images, will allow
more precise measurement, with significantly higher throughput capacity, of retinal
architecture in live teleost ocular tissue.

1.2 Overview of the visual system

The visual system plays an important role in general health assessment and, because of its unique interface with the field of optics, serves as the basis of several disciplines including science and medicine (Whatham et al., 2014 [2]). In order to ethically experiment on the visual system, model organisms are used as the retinas of these model organisms closely resemble their human counterparts. Some common examples of this are the use of rodent retina and, most commonly, mouse retina (Glickfeld et al., 2014 [3]). However, the visual systems of some non-mammalian vertebrate species are relatively understudied at the multi-dimensional imaging level. Spectral domain-optical coherence tomography (SD-OCT) has become an essential methodological approach to study the ocular tissues in live mammalian subjects (Bianco et al., 2019 [4]; Dysli et al., 2015 [5]; Srinivasan et al., 2014 [6]). In the last several years, the use of SD-OCT to study ocular structures of teleosts such as zebrafish (Bell et al., 2016) [7] and more recently lumpfish (Ahmad et al., 2019) [8] has emerged. The use of automated medical imaging technologies to replace manual analytical procedures has become more prevalent in the field of biomedical research (Wu et al., 2017 [9]; Linderman et al., 2017 [10]). Segmentation analysis of SD-OCT images, one of the automated analytical tools currently available for SD-OCT of mammals, allows precise measurement of the different anatomical layers of the retina and is now needed for non-mammalian species as a measurement tool for assessing retinal development, health and disease. Without automated retinal segmentation analysis, the process

of SD-OCT image analysis from non-mammalian species is a labor intensive, manual process (Toms et al., 2017 [11]). In human retinal SD-OCT can be used to identify ocular pathology with neurodegenerative diseases (Chhablani et al., 2018 [12]) such as Alzheimer's disease (AD), Parkinson's disease (PD), Huntington's Disease (HD) and Multiple Sclerosis (MS) (Doustar et al., 2017 [13]; Vuong et al., 2017 [14]). This is especially relevant given the possibility of combining retinal markers with automated SD-OCT systems and software which could be capable of diagnosing and monitoring ocular pathology and diseases associated with it.

1.3   Importance of retinal OCT

Lumpfish (*Cyclopterus lumpus*) are North Atlantic teleost fish that are becoming an important cleaner fish species in salmon aquaculture (Bolton-Warberg, 2018 [15]; Brooker et al., 2018 [16]; Powell et al., 2018 [17]). The visual system of lumpfish is important for both their survival in the wild and for farmed salmon lice removal. Lumpfish have recently been declared threatened in the wild (Lorance et al., 2015 [18]; Committee on the Status of Endangered Wildlife in Canada (COSEWIC), Government of Canada [19]). Therefore, new knowledge on the physiological systems lumpfish rely on for sensing their environment could be important for better understanding this species. Until recently, the visual system of lumpfish was not characterized. A recent study described that cultured lumpfish harbour several features in their eyes that set them apart from other teleosts and mammals (Ahmad et al., 2019 [8]; Paradis

et al., 2019 [20]). Most surprisingly, the study found that lumpfish possess unique retinal anatomical partitioning patterns. The study has also presented the first SD-OCT imaging data from lumpfish retina (Ahmad et al., 2019 [8]). However, the data analysis and the retinal segmentation software accompanying SD-OCT instrumentation is specific to mammalian retina and cannot be used to analyse retinal tissues from teleosts such as lumpfish or cunner(*Tautogolabrus adspersus*) (a western North Atlantic wrasse). In addition, Zebrafish (*Danio rerio*) is a fresh water teleost species that is recognized for its utility as a model organism, fully defined genome and ease of culture (Ribas et al., 2014 [21]). Similarly to lumpfish, the visual system of zebrafish is important for both their survival in the wild and in culture. SD-OCT systems have been applied to zebrafish (Collery et al., 2014 [22]), but retinal segmentation software built specifically for this or other teleost species is currently not available.

1.4   Importance of retinal segmentation

The segmentation of the retina is a non-invasive assessment of retinal structure performed on live subjects to allow researchers to make a quick assessment of the overall health and integrity of both the retina and related anatomical visual system components. This procedure is impactful in research as the representation of perturbations in the different layers of the retina could be indicative of retinal diseases or disorders. In this case, the application of retinal segmentation is important to create new knowledge of the visual systems of teleosts and how these systems relate to previous

research in retinal biology [20].

1.5 Challenges associated with OCT imaging and segmentation

The default proprietary segmentation algorithms provided with commercially available OCT imaging devices are not suited to the task of scanning and interpreting non-mammalian retina. This is the case as most retinal segmentation algorithms display a lack of robustness (Tian et al., 2015 [23]) and are highly sensitive to speckle noise and poor image contrast. These factors combined with the differences between species exemplify the difficulties of creating a universal segmentation algorithm. To overcome the problems of speckle noise and low contrast images, image pre-processing must be used to ensure the accurate detection of retinal boundaries within the image. Pre-processing methods take the form of filtering and smoothing the image to remove as much speckle noise as possible before thresholding. Where tresholding can defined as a binary cutoff value to create a split in image features and can be used to increase image contrast. These techniques serve to add robustness and aide in increased accuracy and reliability of retinal OCT segmentation algorithms.

1.6 Potential approaches to retinal segmentation

In the study of computer vision there are two schools of thought, traditional static heuristic methods and new adaptive artificial intelligence methods. Heuristics, in this case, is defined as fixed mathematical procedures for evaluating the retinal layers. In comparison, the artificial intelligence approach is determined by defining the individual feature characteristics of the retina through rapid evaluation and change over large data sets. After evaluating a number of these procedures, I decided that to solve the problem of applicability, a straightforward approach which made use of the common logic of manual measurements could be created. I determined this to be the best option as it had adaptability of heuristics algorithm and needed much smaller data sets when compared to a machine learning approach. Therefore, thresholding was chosen to build a replacement of manual measurements performed by an expert investigator while keeping the mathematical basis of the solution simple through the column-wise application of replicated manual measurements.

1.7 Aim of the thesis

To address the lack of automated segmentation analysis of SD-OCT imaging data from teleosts including lumpfish and zebrafish, I describe herein the development and implementation of a novel computer algorithm for quantitative analysis of large volume ocular SD-OCT imaging data. This tool differs from other retinal segmenta-

tion algorithms in that it was created for the purpose of segmenting non-mammalian species. This algorithm uses thresholding instead of the traditional use of graph theory or neural network-based methods. This method was designed to interpret individual images and provide the user a new perspective of retinal segmentation. I hypothesized that such algorithms will allow more precise measurements, with significantly higher throughput capacity, of retinal architecture in live teleost ocular tissues. This novel program would create a new research tool to study the ocular tissues of teleosts.

1.8 Organization of the thesis

Chapter 1: Introduces us to the process of retinal segmentation analysis and its core concepts which covers both the challenges and opportunities associated with retinal OCT image segmentation.

Chapter 2: Describes the background of the study of retinal disease and the different approaches that have been implemented towards the segmentation of retinal OCT images with subsections describing different approaches including graph theory and machine learning.

Chapter 3: Describes the methodology used in the automated segmentation analysis of teleost retinal OCT images. It discusses the dataset which was prepared for use in this study, the segmentation algorithm's procedures and its implementation. It also describes error prevention measures that were used to ensure the accuracy of the

produced results.

Chapter 4: Introduces the methodology in which the algorithm is compared against, what is considered the gold standard, manual segmentation performed by an industry expert.

Chapter 5: Concludes the thesis with a review of the algorithms significance and proposes future possible directions of investigation.

Chapter 6: Contains supplementary material which includes a representative spread-sheet output as well as user manuals for the software.

Chapter 2

Literature Review

2.1 Comparison of retinal architecture

To facilitate experimentation on the visual system, model organisms are used as the retinae of some species closely resemble their human counterparts. This common practice can be seen in the popular use of mouse retina (Glickfeld et al., 2014 [3]), in this case we will be using lumpish retina (Ahmad et al., 2019 [8]). To compare the structure of human and lumpfish retina histological sections of retina of each species was presented in Fig 2.1. The histological sections presented were stained with hematoxylin and eosin. The human specimen was sourced from High Resolution Imaging in Microscopy and Ophthalmology [24]. The lumpfish retina images were produced by Dr. Paradis and Dr. Gendron. The images shown in Figure 2.1 displays the similarities between these two retinae in their structural resemblance through the
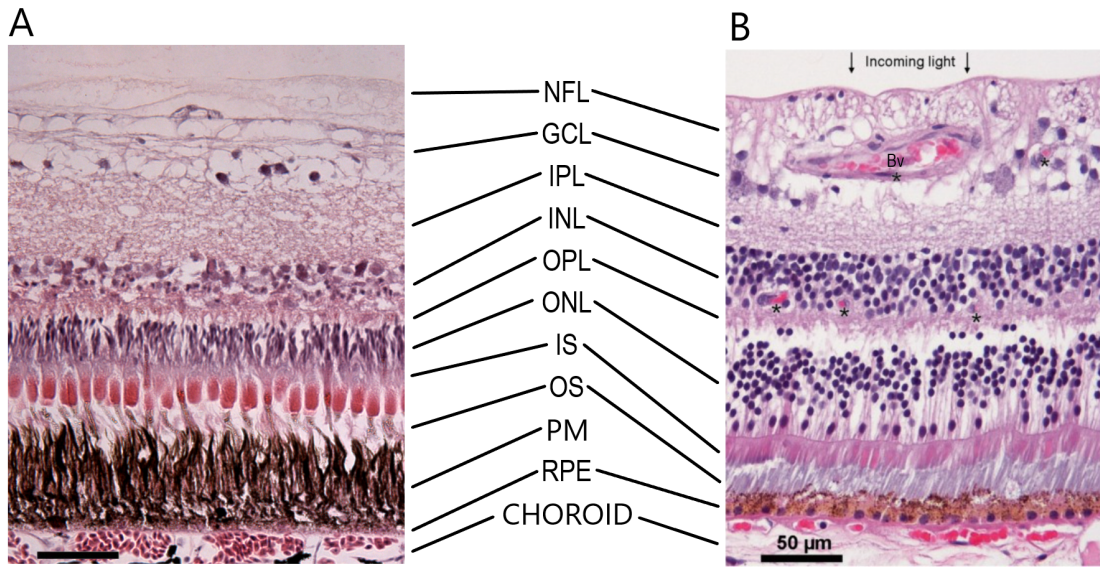
Figure 2.1: **Representative histological sections of lumpfish (a) [24] and human (b) retina with labeled retinal layers.** This includes the nerve fiber layer (NFL), the ganglion cell layer (GCL), the inner plexiform layer (IPL), the inner nuclear layer (INL), the outer plexiform layer (OPL), the outer nuclear layer (ONL), the inner photoreceptor segments (IS), and the outer photoreceptor segments (OS), Pigment (PM) lumpfish only and the retinal pigment epithelium (RPE). The scale bars in both images representing 50 micrometers.

identification of each of the present retinal layers.

In this analysis we can see some great similarities between the human and lumpfish retinae with subtle differences in specific segments. The retinae of both species are very similar for the layers of neural retina (NFL to OS) with the greatest difference occurring in the (RPE to Choroid) section. One example of this was the blood vessels contained in the GLC of the human retina present in the lumpfish retina. In addition to this, the lumpfish contains a pigment layer between the OS and RPE

that was not present in the human retina. This side by side comparison was useful in suggesting a direct structural similarity between both retinae for the purpose of retinal segmentation. In this case similar layers offer us the chance to properly measure and evaluate how the retina was affected by disease and other environmental factors.

2.2   Overview of retinal disease.

Diseases affecting the retina have many different causes and diagnostic procedures designed to asses them are diverse. In this review, the diagnosis of disease was determined as a direct result of the monitoring of thickening or thinning (degeneration) of specific retinal layers. The following overview presents the use of SD-OCT imaging in the evaluation in the development and progression of specific retinal conditions. This knowledge was useful as it shows the potential use of automated SD-OCT software for better understanding the tissue structural changes underlying retinal diseases.

In [13], Doustar (2017) proposed that neurodegenerative diseases such as Alzheimer's and Parkinson's disease can be evaluated through the use of SD-OCT analysis of the retina. This technique was devised to take advantage of the fact that both the retina and the brain were pathologically affected. This paper shows examples of hallmark pathology in the retina for Alzheimer's and Parkinson's as well as Huntingtons Disease (HD) and Multiple Sclerosis (MS). These features manifested themselves in the thickening and thinning of certain areas of the retina which reflects the physiological changes associated with these diseases. While the authors noted that the relationship

between the pathology of the retina and brain was strongest with AD, where the nerve fiber layer (NFL) was thinning. This review shows the potential application of SD-OCT technology in assessing risk and disease progression of neurodegenerative diseases in patients. This paper proposed that this solution could be a cost effective method as it does not require the use of brain amyloid imaging suggesting this solution has the potential to have a great impact.

In [14], Vuong (2017) proposed the correlation between retinal OCT measurements of the ganglion cell complex with visual field defects from optic chiasm impressive lesions. The authors proposed that considerable visual recovery was possible in patients affected by optic chiasm impressive lesions whose treatment was monitored with retinal OCT. The authors also suggest that despite this possibility for recovery the residual damage to the retinal may be more extensive than previously reported. The authors also suggested that ganglion cell complex preservation was associated with better postsurgical outcomes and recovery of the visual field. This paper was an excellent example of new measurement technologies providing new opportunities for the continued development of medical treatment plans. The widespread documentation of an examination of OCT data in the future could create more mainstream retinal evaluations and clinical diagnostic approaches. In the future, more research of this type is critical in the introduction of OCT as a mainstream diagnostic method.

In [12], Chhablani (2018) proposed that interior retinal degeneration could be the earliest sign of neurological diseases. This paper reviews a varying spectrum

of systemic diseases including neurological diseases, hematological diseases, cancer related retinopathies and systemic drug toxicity. The authors found that in the reviewed cases the OCT imaging findings were useful to predict the probability of disease, early diagnosis and to differentiate between healthy and unhealthy tissue and to monitor the effect of therapeutic intervention in many diseases. This paper improved on previous knowledge as they evaluated the viability of retinal therapies in conjunction with OCT technology. However, the authors noted that there remain some challenges in the extrapolation of quantitative data for direct use in clinical intervention. This paper shows that the potential of the retina as an evaluation of health that can be useful for a number of diseases when used with OCT imaging.

In [25], Cassles (2018) reviewed the use of microperimetry in assessing the visual function in age-related macular degeneration (AMD). The authors reviewed 52 articles in which the quality of the analysis was varied to better understand the utility of the technique. The review shows that this method was, at the moment, inconsistent and the authors further suggest its use alongside OCT to enhance the quality of the evaluation procedure. In future studies, this combined procedure could possibility provide a better evaluation approach than traditional methods. This inconsistency originates from the observational design of most of the studies where the risk of selection bias, information bias, or confounding bias may be present. Future studies combining quantitative OCT might entail the ability to process and measure larger amounts of data at a faster rate. This would provide scientists with the opportunity

to perform larger studies with reduced bias as well as document the quality of the assessment technique.

In [26], Costello (2018) proposed that OCT imaging of the retina can be used to measure axonal damage and neuronal loss in Multiple sclerosis (MD) patients. The authors further suggested that OCT detected decrements in retinal nerve fiber layer, ganglion-cell layer and the inner plexiform layer thickness which represent markers of axonal damage and neuronal injury was correlated with worse visual outcomes and increased clinical disability. This paper proposed that with advancements in technology of the differentiation of individual layers through the use of retinal segmentation will allow researchers to quantify the acute and chronic effects of central nervous system lesions. This suggests that future research into neurodegenerative diseases could benefit from the quantifiable measurement that OCT provides to give researchers a better picture of the role of retinal health in disease evaluation.

In [27], Chung (2019) reviewed the role of inflammation in diabetic macular edema (DME) through OCT macular analysis. The authors suggest that inflammation has an important role in the pathogenesis of DME and determined that future research was needed to determine its sub-types. The authors determined that inflammation had an important role but the results were quite different among the different DME phenotypes. This paper describes the potential use of OCT based technology in the research of retinal disease as a method of quantitative evaluation. The review of OCT based treatments was recommended by the authors for the evaluation of future

testing programs.

In [28], Huang (2021) presented a systematic review and meta-analysis on the pattern of peripapillar nerve fiber layer (pNFL) thinning in Parkinson's disease (PD) patients. This review contained the results of thirty-two studies and thirty-three sets of data which involved 2126 PD eyes and 2318 healthy control eyes. This review identified an OCT based biomarker that can be used for differential diagnosis of Parkinsons based on specific patterns of retinal thickness. The authors have identified that certain quadrants of the pNFL were affected differently with the greatest amount of thinning taking place in the inferotemporal segment. This new biomarker can be combined with OCT imaging in the future to create a novel testing environment to potential monitor diagnosis and disease progression.

In [29], Waisberg (2021) reviewed the non-glaucomatous causes of optic nerve cupping or enlargement of the cup-to-disk ration which was a widely recognized feature of glaucoma. In this paper, the authors proposed that the OCT measurement of the retinal nerve fiber layer, ganglion cell layer and inner plexiform layer could be helpful in localizing the disease. The authors describe cupping as consisting of two main components: prelaminar and laminar thinning. Prelaminar thinning was shown to be related to the loss of retinal ganglion cells whereas laminar thinning involved damage to the lamina cribrosa and peripapillary scleral connective tissue. This diagnostical and evaluation procedure serves as a basis for future research into the OCT evaluation of retinal cupping and optic nerve disorders.

In [30] Lee (2022) proposes that progressive parafoveal thinning and fovea avascular zone remodelling, as measured by OCT, could provide a useful biomarker for early diagnosis and prognostication in Parkinsons disease (PD). The authors found that inner retinal changes can be found in the early stages of PD with the macula and peripapillary nerve fibre layers being affected at later stages. With the later being associated with visual hallucinations and cogitative impairment. This paper improves on previous results as a further connection was made between the degeneration of the retina and pathology in the brain. The future widespread mainstream adoption of OCT retinal evaluation could provide high quality information for integrated treatment and monitoring programs.

2.3   Overview of SD-OCT image segmentation.

The process of SD-OCT image segmentation was the task of identifying and measuring each retinal layer in an input dataset and recoding these measurements for later interpretation in research or clinical use. To perform this task several techniques have been developed, some relying on heuristics while others on machine learning technology. With each of these techniques being developed for a specific type of SD-OCT dataset which may include the species and the number of layers to be processed. The general segmentation process consists of image loading, pre-processing for both images and for settings, processing each image in the dataset and returning and formatting the results to be compared. Two main styles of segmentation emerged,

2D segmentation which only considers one image at a time and 3D segmentation which tries to interpret many images as a section of the viewing volume.

Over time, there have been several automated segmentation algorithms, which have been developed to meet the challenge of distinguishing the retinal features needed for a given study. Algorithms are based on kernel optimization (Mishra et al., 2009 [31]), active contour approach (Yazdanpanah et al., 2009 [32]), and graph theory (Yang et al., 2010 [33]), among non-machine learning solutions. In the field of machine learning neural networks (Ronneberger et al., 2015 [34]) have been used in combination with graph search and classification algorithms (Fang et al., 2017 [35]). The main difference between traditional graph-based algorithm and machine learning was the comparison between a constant interpretation and a potential learned response.

2.4 Introduction to graph theory-based retinal segmentation algorithms.

In computer science, graph theory was defined as the study and use of graphs which was a mathematical structure to study the pair relation between objects in a group or collection (Riaz et al., 2011 [36]). In the context of computer science this would refer to the connection of nodes or vertices and edges that connect pairs of nodes. In the case of image segmentation, we will be dealing with the concept of undirected

graphs which are sets of vertices that do not have an order or a given direction. In weighted undirected graphs each edge can be represented by a real number to define its connection with its associated edges.

In the case of image segmentation (Dufor et al., 2012 [37]), we would consider the input image to be an undirected weighted graph, where each pixel value would be represented by an individual graph point which would correspond to an interconnected network of corresponding weighted edges. The process of image segmentation operates on the separation of the graph into two distinct sets. This operation was performed based on the given weighted edges which serve to represent the similarity between a given pixel and its neighbors. Other nodes are often used to represent different types of possible image features or characteristics in addition to the nodes representative of the original image. In retinal segmentation algorithms, additional nodes are added to aide in the differentiating and measuring of retinal architecture.

2.5   Review of graph theory-based retinal segmentation algorithms.

In [38], Garvin (2008) proposed a 3D graph search algorithm to segment five intraretinal layers of the human retina with no other species being mentioned. This process was proposed as one of the first attempts at a 3D segmentation of the total retina. This technique was devised to take advantage of contextual information when

compared to previous attempts. This was achieved using three separate procedures which consist of a scan alignment, composite image creation and intralayer segmentation. The scan alignment and composite image creation combine multiple successive frames into one composite image to include the 3D context of the retinal in a 2D image representation. The intralayer segmentation procedure makes use of points of interest to identify potential retinal boundaries. These potential boundaries are then processed by a cost function to determine their precise location. The algorithms results were then verified with the comparison to manual measurements verified by human experts. This experiment showed the potential of the 3D approach to retinal segmentation but also demonstrated the limitation of the 3D context as it relies on image representation to be properly interpreted.

In [31], Mishra (2009) proposed an adaptive kernel-based algorithm to segment the intra-retinal layers in rodent. This process was proposed as attempts to achieve accurate segmentation under low image contrast and in the presence of irregular features. This technique was used to process both healthy and diseased rodent retinas. This was achieved through sparse dynamic programming where the retinal layers are located, first using estimators to locate their approximate location and then a series of optimization procedures are used to determine the location of the retina boundaries. Where the estimators are used to calculate the potential of a given pixel pertaining to a retinal boundary before the second uses these points to determine the precise location of each boundary. This twostep process was used to avoid the impact of

speckle noise and image artifacts. These algorithms results were then verified with the comparison to manual measurements which shows its potential application to other SD-OCT problems.

In [32], Yazdanpanah (2009) proposed an active contour approach to detect four intraretinal layers in OCT images acquired from rodent models of retinal degeneration. This procedure serves to adapt ChanVeses energy-minimizing active contours without edges [38] for OCT images. This procedure attempts to overcome the issue of low contrast and noise corruption found in ChanVeses procedure. This was done by adopting a cyclical multi-phase framework prior to segmentation to estimate the shape parameters using Least Squares. The Least Squares procedures was used to provide a contextual schema and to balance the weighting of each of the terms in the energy sequence. This was accomplished using both a region based and shape energy term followed by a regionalization energy term to take the average results of the shown 2D context. This procedure shows the potential of image frameworks which combine the use of multiple separate procedures to reduce the possibility of error. The results from various synthetic experiments and segmentation results on 20 OCT images from four rats were presented and compared to manual measurements.

In [33], Yang (2010) proposed an edge detection algorithm based on gradient information and a shortest path search. This was proposed to avoid the possible errors caused by local absolute intensity values, which can be avoided if the layers remain distinct. The gradient information was obtained from the local canny edge result and

the global axial intensity gradient. This was used to determine nine retinal boundaries sequentially so that previous information can be used. This was accomplished by building and modifying a graph generated with the canny edge detector using the axial intensity gradient to provide additional information, then the shortest path was used to determine the boundary location. This algorithm was used to process human retinal imaging data consisting of glaucoma and control patients and were compared with manual segmentation. In the future, more work will be needed to evaluate the approach of retinas affected by different physiological change associated with retinal disease.

In [37], Dufour (2013) proposed an edge detection algorithm based on gradient information and a shortest path search. This was proposed to avoid the possible errors caused by local absolute intensity values, which can be avoided if the layers remain distinct. The gradient information was obtained from the local canny edge result and the global axial intensity gradient. This was used to determine nine retinal boundaries sequentially so that previous information can be used. This was accomplished by building and modifying a graph generated with the canny edge detector using the axial intensity gradient to provide additional information, then the shortest path was used to determine the boundary location. This algorithm was used to process human retinal imaging data consisting of glaucoma and control patients and were compared with manual segmentation. The authors stated that, more work will be needed to evaluate the approach of retinas affected by different physiological change associated

with retinal disease.

In [39], Duan (2018) proposed an automatic graph-based multi-surface segmentation algorithm that internally uses soft constraints to add prior information from a learned model. This method was proposed to improve the accuracy of graph-based segmentation through increasing its robustness to noise. This method also attempts to reduce the size of the graph being considered by applying a segmentation scheme. This was accomplished through the building of a prior information model to enhance a graph-based segmentation model. In this case the information model was a statistic on the distance between surfaces in relation to the fovea position which was composed of multiple mean models. This model was then used to shape the segmentation input to reduce the total graph size. The method was verified on twenty human OCT datasets of healthy eyes. These scans were then compared to manual measurement and reviewed by human observers. This procedure shows the importance of graph size reduction [33] in retinal segmentation.

In [40], Bekalo (2019) proposed an algorithm to both segment the layers of the retina and the sub-retinal fluid often associated with neurosensory retinal detachment (NRD). This algorithm was based on the use of graph search and graph cut methods to segment the input viewing volume as a 3D fully automated procedure. This algorithm contains three main parts, a prior information model, a fluid segmentation and a layer segmentation. To reduce the computational cost of graph-based optimization, a "divide and merge" approach was used. The prior information model used both soft

and hard smoothness constraints to add prior information from a learned model, which was used to increase its robustness to image noise. Finally, the layer segmentation takes the form of stratified sampling which used Adaboost in conjunction with multi-scale graph search and shape-constraint graph cut methods. This algorithm was tested on human SD-OCT cubes diagnosed with NRD, and the results were compared with the manual segmentation results from experts. This algorithm suffers from its high complexity but showed its potential application to other SD-OCT problems.

In [41], Lou (2020) proposed a graph-based wave algorithm to segment the layers of the human retina. This algorithm was comprising of an OCT enhancement method based on averaging sequences of images followed by an edge detection method based on custom wave algorithms. These two separate images are then fused together using an image fusion sigmoid energy conservation equation to generate the final enhanced image which displays the retinal layers. This solution was proposed to overcome the problem of speckle noise and low contrast images. In this example down-sampling and filtering was used to remove speckle noise from the image and a fluid potential energy equation was used to segment the retina. This program was tested against similar methods running their test dataset of human retinal OCT images. This algorithm provides an example of interchanging demonising and segmentation methods to account for image quality.

In [42], Ma (2021) proposed structure interpolation and lateral mean filtering (SI-LMF) algorithm to improve the signal-to-noise ratio based single image processing.

This process consists of one-dimensional lateral mean filtering to remove noise, structure interpolation to eliminate thickness fluctuations and a boundary growth method. This algorithm was based on human retina and attempts to identify the boundaries of ten physiological layers. This proposed method does not rely on the processing of multiple images at a time and lowers the computational cost of the algorithm. The algorithm was tested on human OCT images and was compared to manual segmentation analysis. The algorithm provides an example of the future potential of a hybrid approach to solve problems in SD-OCT image processing involving the use of both traditional methods and machine learning.

2.6 Strengths and weaknesses of graph theory retinal segmentation

The strengths of graph-theory-based segmentation are its reproducibility and adaptability. As the math underlying these segmentation methods was in the form of heuristics, it can be reproduced and verified according to mathematical logic. This logical evaluation aids for adaptability as the underlying solution can be both applied to newer forms of technology and expanded with new adaptions for specific problem sets. This technology was especially relevant as there are many problems in retinal segmentation where little data exists. In these situations the applicability of a current method would be the optimal solution. As the goal of graph theory-based segmenta-

tion was to identify the retinal layers through the identification of connected paths where, it can often prevent the correct retinal layers being identified due to harsher image artifacts, sparkle noise or other features. Another weakness of these algorithms its there tendency to round the solution has the path is being drawn meaning that earlier mistakes in these paths can through off the segmentation procedure.

2.7 Introduction to machine learning based retinal segmentation algorithms.

In computer science, machine learning would refer to the creation of algorithms and data processing techniques that would be able to improve the result of a given task as more input data was processed. In the example of image segmentation these processes are used to identify and measure the corresponding retinal layers using neural networks. A neural network was a circuit used to represent the biology of the human brain and consists of several connected layers. The given weights associated with the given connections and their associated node activation functions determine the potential output of the system. Hence, the adjustment of the weight and biases from processing data adjust the system to suit its input dataset. In retinal segmentation, the whole image was input into the neural network system which will attempt to determine the location of the individual retinal layers. Different types of neural network structure and activation functions can be used to adjust the algorithm settings

in order to understand different problem types.

2.8 Review of machine learning based retinal segmentation algorithms.

In this section we will be summarizing some of the different machine learning based SD-OCT image segmentation algorithms.

In [43], Lang (2013) proposed the use of an automated approach to approximate nine individual retinal boundaries through the use of a random forest classifier. This classifier operated on macular cube images reconstructed from retinal OCT data and used this information to construct a probability map for each boundary. The random forest classifier learns the boundary pixels between retinal layers and produces a probability map for each boundary which was processing into the final boundaries. The images are pre-possessed with an intensity normalization procedure before being processed by the boundary classifier. This algorithm was tested on both healthy and multiple sclerosis subjects and was compared to manual measurements. In future modifications of the process, it will be necessary to handle other ocular pathologies such as microcysts, drusen, and geographic atrophy (GA). This algorithm showed the potential of the use of image classifiers to identify the retinal layers of human retina without the use of deterministic segmentation.

In [34], Ronneberger (2015) proposed a system of convolutional networks for

biomedical image segmentation (U-Net). This method presented network training strategies that rely on data augmentation to use annotated samples more effectively. This procedure was devised to overcome the limitation of sparsely trained neural networks. The network uses a system of both a contractive and expansive path. This system presented the possibility to make better use of small datasets when training, but with that comes that possibility of training bias. This method has been adapted for use in retinal segmentation and was used as the starting point for many machine learning based algorithms. The use of the network architecture when combined with an extensive framework could possibly, in the future, produce a valuable opportunity for experimentation. However, its real-world application could be limited by the available amount of annotated data. The cost of specific training hardware for the development and use of the software can be resource intensive. Therefore, the application of the algorithm could provide future opportunity for expansion but its implementation would come at a high data cost.

In [35], Fang (2017) proposed a framework based on combining convolutional neural networks (CNN) and graph search methods. This combined procedure first used a CNN to extract features of specific retail layer boundaries and train a corresponding classifier to delineate a pilot estimate of the eight layers of human retina. The first step consists of an image pre-processing routine followed by a CNN method to extract features and label them according to the retinal layers being interpreted. This was followed using graph search methods to determine the location of each of the retinal

layers. This algorithm attempts to avoid specular noise and image artifacts by adding an additional label to the CNN which was trained to classify pixels that are deemed outside the retinal boundary. This process was validated on sixty OCT image volumes (2915 image B-scans) from twenty specimens with non-exudative age-related macular degeneration (AMD). These procedures show the use of CNN for the elimination of image noise and artifacts from OCT images for use in segmentation.

In [44], Roy (2017) proposed a fully convolutional neural network which uses contractional paths of convolutional blocks (encoders/decoders) to learn a hierarchy of contextual features. The process attempts to both segment the retinal layers and the fluid masses contained in OCT scans. The process the algorithm takes is to construct custom pooling procedures to identify and segment five retinal layers, before reporting the total loss and retuning the results. The algorithm was tested on Duke SD-OCT publicly available dataset for human DME patients and compared with manual measurements. This algorithm was proposed to show the importance of skip connections and joint loss function in the field of neural networks. However, very large amounts of data are needed to properly train the neural network and its computation would consume a large amount of computing power which would be time consuming.

In [45], Montuoro (2017) proposed a retinal layer and fluid segmentation OCT algorithm to process human retinal data with severe macular edema. This was a fully automated 3D process which combines the use of both machine learning and graph

theory methods. An unsupervised feature representation was used to determine the location of the retinal features present in the input dataset. Followed by the use of special context methods and graph theory to perform a surface segmentation analysis. This procedure first determines the context of a given pixel then calculates the retinal boundaries based on their relative position. This procedure was built to overcome the difficulties of fluid accumulation in OCT imaging. This method was tested on manually annotated segmentation analysis of image scans of ten human patients with severe macular edema.

In [46], Wang (2017) proposed an algorithm which uses the Markov random field and Level-set method to segment the choroidal layer of the human retina This method works by first using 3D nonlinear anisotropic diffusion filter to remove speckle noise and increase image contrast. The level set method was then used to apply distance regulation to avoid local irregularities and to have a clear separation between the choroid and sclera. Markov random field was then used to determine the single pixel likelihood with neighborhood information to compensate for image texture and to avoid errors along the edge of the boundary. This method was then compared with a dataset with manually labelled ground truth. This method shows the potential of 3D filtering in retinal segmentation analysis and the use of field equations in specific retinal segmentation. In the future, more work can be done to combine specific segmentation algorithms into a larger segmentation framework.

In [47], Shah (2018) proposed a convolutional neural network (CNN) based frame-

work to segment multiple surfaces simultaneously. This proposed method uses a single CNN to segment three retinal surfaces. The algorithm was trained to process both normal retinas and retinas affected by intermediate age-related macular degeneration (AMD). The algorithm was designed to overcome the large computing costs of graph based optimal surface segmentation and a "U" structured convolutional networks system for biomedical imaging systems (U-Net) [34] based methods. This method was validated on fifty human retinal OCT volumes (3000 B-scans) including twenty-five normal and twenty-five intermediate AMD subjects. The algorithm was then compared to be an improvement over the optimal surface segmentation method with convex priors (OSCS) [48] and two deep learning based U-Net methods for both data types. The proposed method shows the potential to be extended to higher dimensions so it can attempt to segment more retinal architecture.

In [49], Borkovkina (2020) proposed an algorithm to segment eight retinal layers of the human retinal using a compressed, low-latency neural network. This procedure attempts to achieve real time segmentation through its use of three different levels of optimization. These optimization procedures consist of a neural network structure, a neural network compression scheme and specialized graphics processing unit (GPU) hardware. This method generated a neural network representation then compresses it before using specialized hardware to process and extract the location of the retinal boundaries. This was then compared with a test dataset consisting of human retinal to the U-Net [34] where it showed an improvement in the speed of the segmentation

procedure. This method shows that the use of specialized hardware can improve the use of neural networks by greatly reducing their latency. The use of this software on conventional hardware could be limited due to its lack of tensor cores, which this method uses to increase in neural network performance.

In [50], Yow (2020) proposed a retinal nerve fiber layer segmentation for use in high-resolution swept-source human OCT. This method uses a deep leaning algorithm which operates using the U-Net architecture [33] which has been modified to suit a nerve fiber layer (NFL) segmentation. In this procedure cross-sectional micropapillary images are extracted and then combined in sets and to be processed as one cumulative image. The results of the algorithm were then compared against expert human manual segmentation on a dataset consisting of both healthy and glaucomatous subjects. This algorithm shows that neural networks can be used for specific segmentation tasks when enough data can be made available and that algorithms can serve as platforms for future experimentation. Moreover, there was scope for further work on reducing the amount of information needed to train and process these specific segmentation networks in the future.

2.9   Strengths and weaknesses of machine learning retinal segmentation

The strengths of machine learning retinal segmentation based algorithms are its robustness to image defects such as speckle noise and image artifacts. The underlying nature of machine learning allows the solutions to process large amounts of data which can in turn allow it to avoid image irregularity when used on large datasets. This gives machine learning algorithms the ability to gain accuracy with the scale of its data input. As a result, machine learning solutions would have to be retrained with a different dataset and internal setting to adaptive itself to a new machine learning task. This necessity of large large data requirements and the difficulty involved in adapting a current working solution to suite other models [51]. As machine learning methods are data heavy solutions this can often prevent their applicability to small datasets and specific problems. The costly nature of both large datasets and the necessary computing power to process them could restrict the overall impact of machine learning based solutions. This can be seen in (Yanagihara et al., 2020 [52]) who looked into the consequence of a lack of large datasets in retinal machine learning.

2.10   Conclusions

We have seen that, over time, researchers have developed various algorithms to address the problem of automatic SD-OCT image segmentation. These techniques all

attempt to better interpret and process retinal imaging of healthy and unhealthy specimens to aide in both diagnostics and research. It was not known if these algorithms can be applied to other species especially non-mammalian species as most retinal segmentation algorithms are primarily designed for mammalian retina. The thresholds method featured in this thesis was chosen to build on the strengths of heuristic algorithms by having a simpler mathematical base making the algorithm approachable to modify to properly suite the retinal characteristics of other species. As the applicability of the algorithm was the goal a machine learning based approach would not be appropriate as each species would require the collection and pre-evaluation of a large amount of data. It was important in the future that algorithms produce reliable results to ensure their continued use in the research setting. We have also seen the various types of diseases that could be monitored using retinal thickness monitoring techniques and how this process was a novel concept in the field of biomedicine. I hope, in the future, algorithms and automated systems can fully replace the need for manual measurements in the retinal segmentation process in all forms of research and evaluation.

Chapter 3

Methodology

3.1 Animals and SD-OCT image acquisition

The data provided for this study was collected by Dr. Paradis and Dr. Gendron using cultured lumpfish from the Department of Ocean Sciences, Memorial University under the approval of the Institutional Animal Care Committee (protocols 17-03-RG; 17-01-RG). Retinae from lumpfish were imaged noninvasively by SD-OCT essentially as described previously (Ahmad et al., 2019 [8]). Lumpfish were randomly selected from three holding tanks of 150 specimens each. Fish were transported from the Dr. Joe Brown Aquatic Research Building (JBARB), Department of Ocean Sciences to the SD-OCT imaging laboratory (Faculty of Medicine) in a cooler box with fresh oxygenated tank water, acclimated for 30 minutes then lightly sedated with 40 to 80 mg/L tricaine methanesulfonate (Sigma, Oakville, ON) in tank water. Tear Gel

(Alcon, Mississauga, ON) was applied to keep the eyes moist. The fish gill areas were wrapped in gauze soaked with tank water and placed in a silicone cradle, with the imaged eye facing toward the SD-OCT bore lens (90-BORE-G4-M G4 Mouse lens). "En face" SD-OCT images were acquired from the live anesthetized animals using a Leica Envisu R2210 SD-OCT instrument (Bioptigen, Durham, NC). Scans were acquired in rectangular volume, 1 X 1000 X 100, 1.8mm X 1.8mm mode. Scans were completed for both the oculus dexter (OD) and oculus sinister (OS) eyes of each animal. Zebrafish SD-OCT scans (rectangular volume, 1 X 1000 X 100 mode were kindly provided by Dr. J. Vance (The Spective Group, Raleigh-Durham, NC). The human dataset was composed by the University of Waterloo Theoretical and Experimental Epistemology Lab (TEEL) [53] which contains 500 high resolution images categorized into different pathological conditions. The image classes include Normal (NO), Macular Hole (MH), Age-related Macular Degeneration (AMD), Central Serous Retinopathy (CSR), and Diabetic Retinopathy (DR). The images were obtained from a raster scan protocol with a 2mm scan length and 512x1024 pixel resolution.

3.2 Manual Image Analysis

Manual SD-OCT image analyses of the retinal thickness was captured using OpenLab [54] software ruler tool on each selected B-scan image. In each of the manually measured images ten relatively evenly spaced measurements were selected to represent the overall thickness of the retina as individual measurements. These measurements

were then saved as separate spreadsheet files corresponding to each specimen. These manual measurements were overseen by Dr. Paradis who is an experienced scientist in the field of retinal research. Dr. Lilly[3] performed the lumpfish segmentation and I performed the zebrafish segmentation.

3.3 Software Availability

The software developed alongside this thesis to demonstrate the mathematical principles of the algorithm will be made available for testing and personal use on all platforms and hosted on a dedicated GitHub page. This software and any future updates will be made available for testing and personal use on the GitHub platform [55] at the following link, https://github.com/krbarter/SD-OCT-Points-Based.

3.4 Program design and implementation

This program was designed through the use of three-tier architecture which consists of input, application and data as three separate layers Fig. 3.1 in conjunction with object oriented program design (OOP) [55]. This program was implemented in the python programming language and made use of packages such as matplotlib, numpy, opencv-python, Pillow, XlsxWriter, xlwt and wxPython. The program's design revolved around a single user interface for input of data and settings into the program, an application layer which performed the algorithm's computations followed by data

processing and output. Both the program's design and implementation were built

with simplicity and user oriented design in mind with the goal of creating a program

that is easy to follow, maintain and update. Our novel algorithm can be illustrated

in terms of a waterfall model Fig. 3.2.

Input

Pre-Processing

- Non-local Means Denoising
- Gaussian Blur
- Median Blur
- Truncated Thresholding

Processing

- Thresholding to find each retinal layer by column
- Store data for later processing

Results

- Processing Data
- Preparing Heatmap Results
- Presenting Heatmap Interface

Output: Results Document and Heatmap
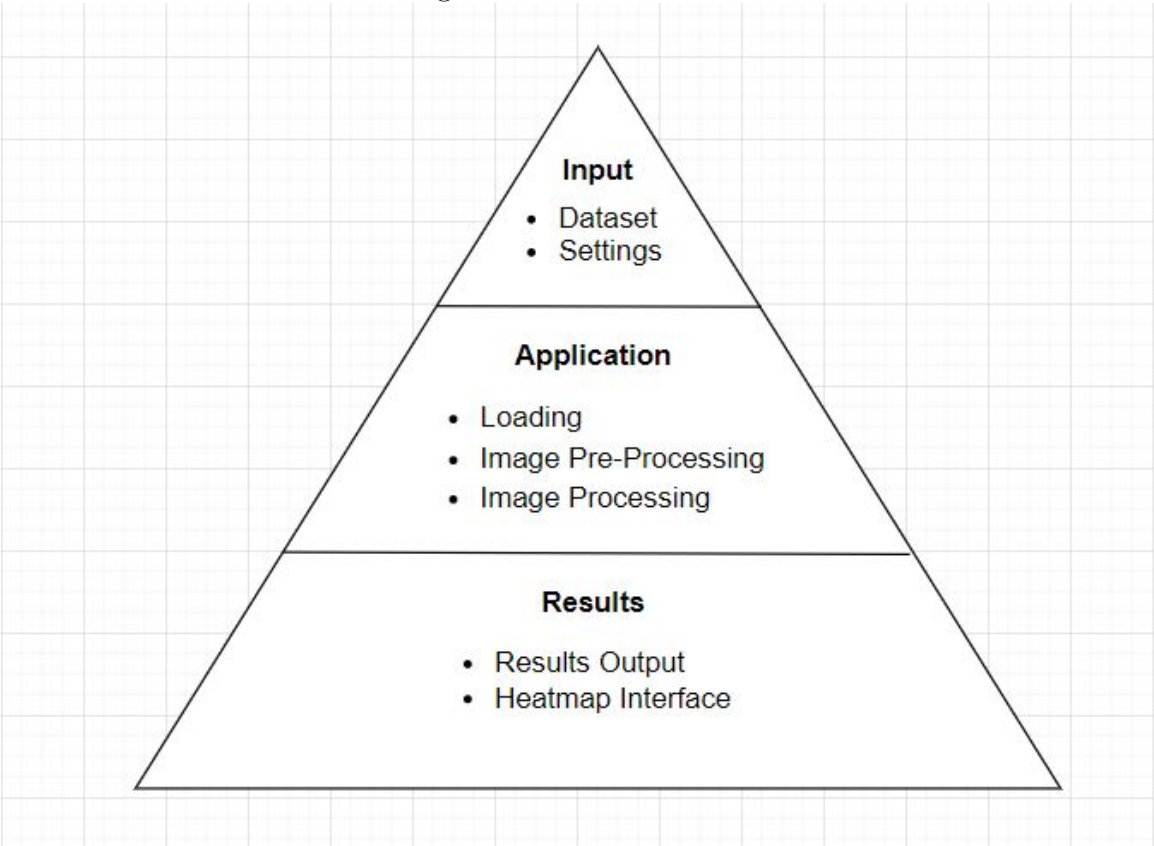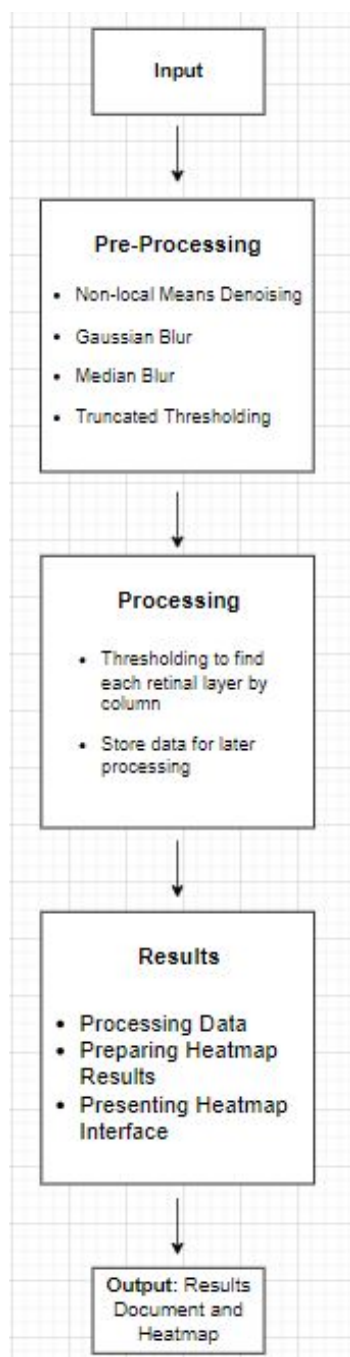
Function: *Pre − processing*;

    Load Images from directory ← Images;

    for *Each Image* **do**

        Non − local Means Denoising;

        Gaussian Blur;

        Median Blur;

        Truncated thresholding;

end

Function: *Processing*;

    for *Each Image* **do**

        for *Each Column* **do**

            Use input thresholding values to determine the outer retina;

            Record each measurement;

    end

end

Function: *Results*;

    for *Each Set of Images* **do**

        Output and display 2D Heatmap;

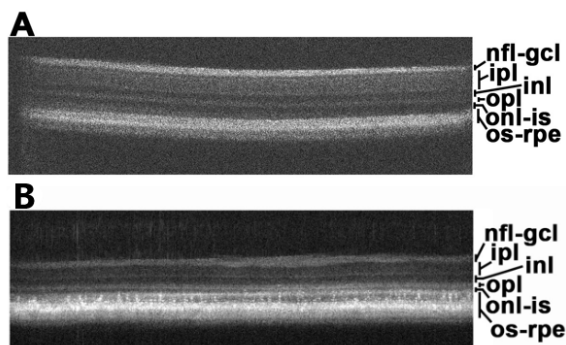   *Output and display 3D Heatmap*;

        Output results spreadsheet;

end

<div align="center">

Algorithm 1: Algorithm Pseudo-code.

</div>

3.5 Retinal Architecture

In the case of retinal segmentation, the measurement of the thickness of specific retinal layers for use in scientific research is of great importance. This was achieved through segmentation analysis of the nerve fiber layer (NFL), the ganglion cell layer (GCL), the inner plexiform layer (IPL), the inner nuclear layer (INL), the outer plexiform layer (OPL), the outer nuclear layer (ONL), the inner photoreceptor segments (IS), and the outer photoreceptor segments (OS) and the retinal pigment epithelium (RPE) followed by data display. In this algorithm we will be identifying several distinct retinal layers of both the lumpfish and zebrafish as shown in Fig. 3.3. The first of these measurements will be the total retinal thickness, with the second being NFL/GCL, thirdly IPL/INL/OPL/ONL/IS in the case of the lumpfish or the IPL/INL and OPL/ONL/IS/OS/RPE as two distinct segments in the case of the Zebrafish ending with the OS/RPE for the lumpfish. These layers have been identified as both important to the study of the retina and applicable to the teleost species included in this solution with several retinal layers remaining unsegmented by this approach.

3.6   Program

An image segmentation program was built using OpenCV (Open Source Computer Vision, 2020 [56]) to analyse and interpret SD-OCT B-scan images to determine the thickness characteristics of the different layers of the retina of lumpfish. The images from a given set of specimens, to be compared to one another, were loaded and processed together (Fig. 3.1). The images were processed by the following three phases, with the result of the previous phase being the input to the next phase. First, images were loaded and refined by excluding image artifacts and eliminating as much noise from the image as possible using Non-local Means Denoising followed by a Gaussian Blur, followed by a Median Blur and Truncated Thresholding. These processes aid to reduce possible error in the identification of the retina and refine the image so that the program can correctly identify the different layers of the lumpfish retina. Second, the refined images were processed using a novel algorithm to find the retina located in the input image. Third, the data was analyzed and output. The overview of this algorithm's procedures can be seen in and (Fig. 3.1 - 3.3) respectively.

The program's image processing algorithm has been based on thresholding, which operates on the pixel values contained in an image where the threshold values are given as user input. Thresholding was accomplished by taking any value that meets a certain requirement and rejecting all others. Three main variables were used to determine the location of the retina and its layers. The first variable represents the minimum acceptable pixel value of white while the second variable corresponds to

the minimum gap between two white pixels and the final variable is the maximum allowed gap between two white pixels. The algorithm functioned by viewing each column of pixels and storing the location of white values that pass the thresholding function. Where white values are defined as values approaching the white side of the gray-scale range. The first and last threshold values of a column of pixels were marked by a blue highlight and delineated the total thickness of the retina (Fig 3.3). The program was designed to then identify a large gap between two white pixels based on the second and third thresholding variables. The last value before the gap and the first value after the gap were marked by a green highlight. The middle of these two points, deemed the smoothing line, was marked by a red highlight and saved as a separate output. This optional smoothing line provided an additional evaluation tool revealing the retinal curvature. The thickness calculations were taken directly from the thickness measurements, which measured and interpreted the data seen in the highlighted columns of pixels on each image. It should be noted that only the highlighted values in each image were measured and excludes all other sections failing to meet one or more thresholding values used in the algorithm. The program can be adjusted by the modification of one or more of the thresholding variables to suit the input image set. The number of measurements made by the algorithm is determined by the number of columns of pixels found by the thresholding algorithm, containing the retina, with the maximum number being the width of the image in pixels. Once all measurements are made the image is then saved, storing the position of all measured

points. In addition to adjustable thresholding variables, to prevent possible error, the program was designed to complete a functional analysis that determines if the retina is missing from the image or if the image contains a large amount of noise or artifacts. This is performed by determining if the image contains the correct number of pixels with a certain intensity above a threshold. In these situations, these images contain too many artifacts and will be rejected and will not be processed by the image processing algorithm. Another feature to prevent false measurements is a minimum measurement thresholding variable, to exclude measurements created when the program chooses the same point or two separate points too close together to represent any retinal structure. As these points are most likely clumps of noise or image defects that are remaining in the pre-processed image.

The program's data analysis component was designed to process the stored image data set into a finished data output. Data output reported the program's internal settings to aide in analytical reproducibility. For each SD-OCT B-scan, the image sequence numbers (referred to as B-scan number) were recorded in the beginning of each data entry. Data output consisted of the mean retinal thickness for each image with the number of points measured for each retinal layer (Appendix 6.1). From these measurements, the thickness of the specific retinal layers of each SD-OCT scan were reported as a percentage of the whole retina thickness (Fig. 3.2 (F)).

The SD-OCT data produced by the image segmentation program was interpreted by a heatmap program designed to represent the relative thickness of the whole reti-

nal SD-OCT scan. This was done by analysing all thickness values produced from a complete set of B-scan images containing scanned specimens. The difference from the minimum value were then colour assigned by the difference in comparison to the minimum value according to a colour scale. The minimum thickness values were represented by blue colour and gradually increase in thickness represented by green, yellow, orange and finally red representing the maximum thickness (Fig. 4.5). Each colour ranged from a grade of one to eleven in intensity to create a colour gradient representing how the program processes of the whole dataset of measurements taken from the total retina thickness for each SD-OCT B-scan. The program plots each measurement as one pixel in width and ten pixels in height assigning it to the appropriate colour setting before saving the produced data as an image, to correctly represent the width of the retina. To avoid error, any value outside the range of the colour gradient was assigned to the bounds of the range. Any value above the gradient was assigned the highest value and any value below the gradient assigned the lowest value.

In addition to the 2D heatmap, a 3D representation of the heatmap data was constructed using a 3D surface map which used the same data and colour range as the original 2D representation. The 3D surface was constructed using a triangular surface mesh which displays the outer surface of the retina which gives the user a better perspective on both the surface of the retina and the shape of the retina in the vicinity of the optic nerve head.

3.7 Statistical analysis

Two-tailed student T-tests were used to analyze the statistical significance of the difference between the measurements of retinal thickness from B-scans assessed manually versus those assessed by algorithm processing. The measurements were considered statistically different if the P values were equal or less than 0.05.

Chapter 4

Results and Discussion

The use of SD-OCT instrumentation in combination with native manufacturer software to analyze teleost retinal parameters such as retinal radius or retinal layers has been reported [16][18]. However, the work herein is the first description of a custom algorithm designed to automate analysis of SD-OCT data to measure retinal architecture in teleosts fish, including marine teleosts. I designed an image segmentation program to scan and interpret SD-OCT retinal B-scan images to determine the overall thickness of the retina and thicknesses of the different sub layers of the retina of teleost. This program enables SD-OCT image analysis to be processed rapidly to provide reproducible SD-OCT data (Fig 4.1, 4.2 (b) and (c)). This clear segmentation of retinal architecture was also provided with a smoothing line to facilitate the visualization of the curvature of the retina (Fig 4.1 (d)).

Figure 4.1: **Representative SD-OCT retinal B-scan analysis from a cultured lumpfish. The original B-scan image (a) was segmented through our algorithm (c).** This segmentation is shown as an overlay of the original image (b) over the original image (a) and as processed segmented image (c) which is labeled with the program's produced average measurements. The segmentation of the lumpfish retinal layers includes the nerve fiber layer (NFL) / ganglion cell layer (GCL); the inner plexiform layer (IPL) with the inner nuclear layer (INL), the outer plexiform layer (OPL) and the outer nuclear layer (ONL) / inner segment (IS); and the outer segment (OS) / retinal pigment epithelium (RPE). This image is followed by the smoothing line output of the segmentation of (a) which is represented by a red line generated by the program segmentation delimitating the middle point of the retinal layers as shown in (d). This is followed by a representative image of a manual segmentation analysis which showed ten manual measurements (e).
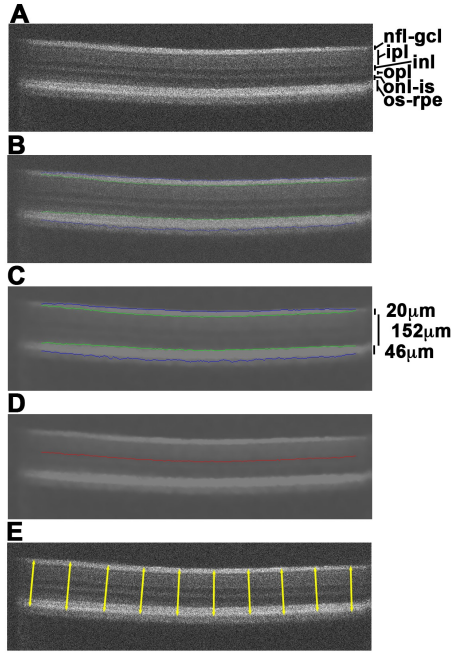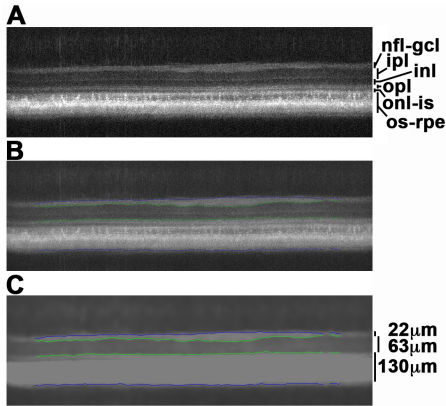
Figure 4.2: **Representative SD-OCT retinal B-scan analysis from a zebrafish. The original B-scan image (a) was segmented through our algorithm (c).** This segmentation is shown as an overlay of the original image (b) over the original image (a) and as processed image (c) which is labeled with the program's produced average measurements. This segmentation of the zebrafish retinal layers includes the nerve fiber layer (NFL) / ganglion cell layer (GCL), the inner plexiform layer (IPL) with the inner nuclear layer (INL), the outer plexiform layer (OPL) with the outer nuclear layer (ONL) / inner segment (IS) and the outer segment (OS) / retinal pigment epithelium (RPE).

I have designed the program to output the retinal layers thicknesses of each SD-OCT B-scan in the form of a data file in the Excel (XLSX or XLS) or Comma-separated values (csv) format. An example of such data file for lumpfish is represented in Appendix, 6.1 Table. This data file contains the retinal layer thickness measurements, the number of measurements or readings per B-scan and internal settings associated with the processing of a dataset. The program output also included the thickness of the segmented retinal layers of each SD-OCT scan as percentage of the whole retina thickness. The retinal thickness measurement analysis of the rep-

resentative juvenile lumpfish eye presented in Appendix, 6.1 Table revealed that the NFL/GCL represents 14.9% of the volume of the retina, while the inner layers with the outer layers and IS volume percentage was 61.9%, and the OS/RPE represented 23.2% of the volume of the retina. The program includes error prevention measures, to ensure data accuracy, and thresholding variables to allow the program to be adaptable to any SD-OCT dataset. Since thresholding is used, any input produced the same output when all settings remained the same. This algorithm is novel as it is the first of its kind to be developed specifically to study teleost. As with any scientific process the elimination of errors is important. The program has several features to avoid possible errors in the interpretation of the retina. These features include the adjustable thresholding methods which can exclude information from being detected and placed into the data. The error prevention techniques including thresholding variables and functional analysis, can eliminate the occurrence of most error from appearing in the dataset. As the program is making hundreds of measurements per B-scan, there can be an acceptable amount of error that would not affect the results. Unlike when manual analysis is used (Fig. 4.1. (e)), using ten measurements per scan, a single error can greatly affect the results. Our program was designed as a replacement for manual analysis of SD-OCT B-scan data of teleosts. This algorithm proved to be a capable replacement for manual segmentation analysis as depicted in the comparison and accuracy analysis performed in lumpfish (Fig. 4.3).

Figure 4.3: **Comparison between manual measurements and the algorithm's segmentation analysis of lumpfish retinal thickness.** Three B-scans per specimen were selected and average retinal thickness evaluated manually using 10 manual measurements or using the algorithm with as many measurements as possible up to the width of the image. Error bars represent the standard error of the mean. No significant differences were observed between the manual versus the algorithm measurements (T-test, $P > 0.05$).
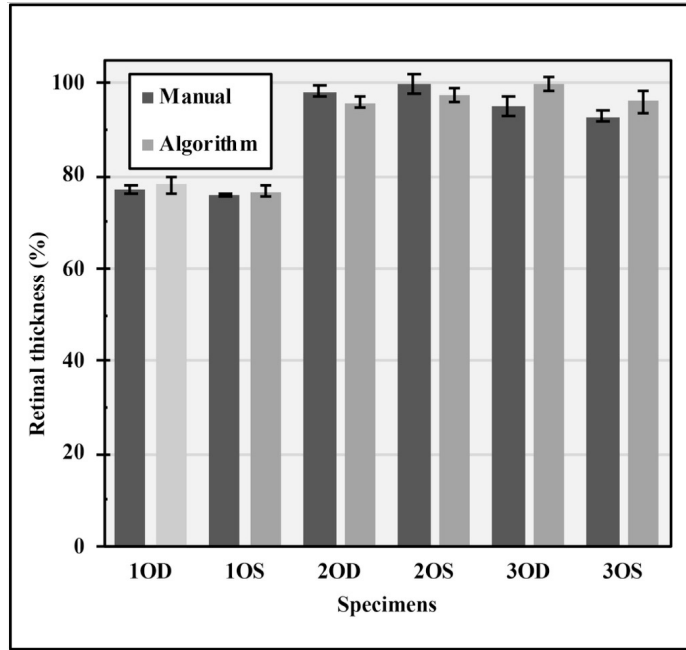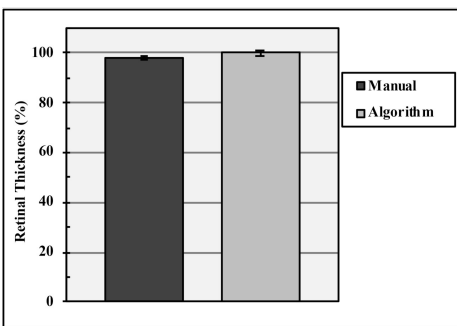
Figure 4.4: **Comparison between manual measurements and the algorithm's segmentation analysis of zebrafish retinal thickness.** Five B-scan images were selected and average retinal thickness analyzed manually with 10 manual measurement and using the algorithm with as many measurements as possible up to the width of the image in this case 2515 total measurements. Error bars represent the standard error of the mean. No significant difference was observed between the manual versus the algorithm measurements (T-test, P > 0.05).

Similarly, the results of manual analysis were compared to the algorithm which showed an equivalence to manual measurements in the corresponding zebrafish B-scans images (Fig. 4.4). Because the algorithm processes information at a faster rate, more specimens can be included in an individual study than using the manual analysis. Having the capacity to be able to process more data and take more measurements per image combined with data analysis the algorithm increases the amount of repeatable SD-OCT data produced from a given set of B-scan images over the manual analysis. Moreover, the turn around time between the production of data and results is greatly reduced with the algorithm.

Additional features of our program include the generation of a heat map representing the relative thickness of the retina throughout the whole SD-OCT retinal

51

scan from individual B-scans. A representative heat map of the whole SD-OCT retinal scan of a juvenile cultured lumpfish aged 100 days post hatch is shown in (Fig. 4.5). The heat map included the specific specimen identifier, the number of B-scans processed and the colour gradient display corresponding to the different levels of retinal thickness. This heat map is particularly useful to visually and rapidly identify areas of the retina displaying different thicknesses. The heat map is also useful in identifying retinal architecture and the position of the optic nerve, which can be seen in the top of the heat map (Fig. 4.5). This was confirmed through analysis of the individual B-scans as seen in (Fig. 4.2). The overlay of the heat map with the volume intensity projection ("en face" image) generated by the SD-OCT instrument demonstrated how the shape of the retina, displayed by the heat map, corresponds to the volume presented in the intensity projection. This demonstrates the relevance of the heat maps in representing the shape of the retina through visualization of its thickness characteristics corresponding to the anatomy seen in the "en face" image.
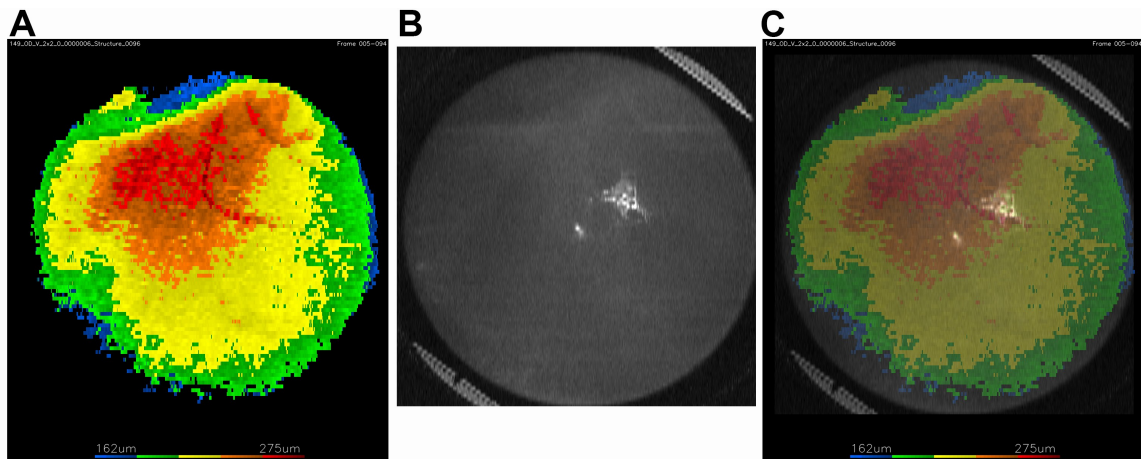
Figure 4.5: **Heat map of a SD-OCT scan of a lumpfish retina. A representative 2D heat map displaying the relative thickness of the whole retina from a complete SD-OCT scan of a 100 days post hath (dph) juvenile cultured lumpfish (a).** The heat map includes the specific specimen identifier, the number of B-scans (frame) processed and the color scale representing the relative thickness in micrometers. The position surrounding the optic nerve can be seen in the heat map as the thinner blue area at the top of the image this was confirmed through analysis of the individual B-scans as seen in (Fig. 4.2. (c)) An overlay of the heat map with the volume intensity projection ("en face" image (b)) of the SD-OCT scan of the same specimen is shown on the right panel.
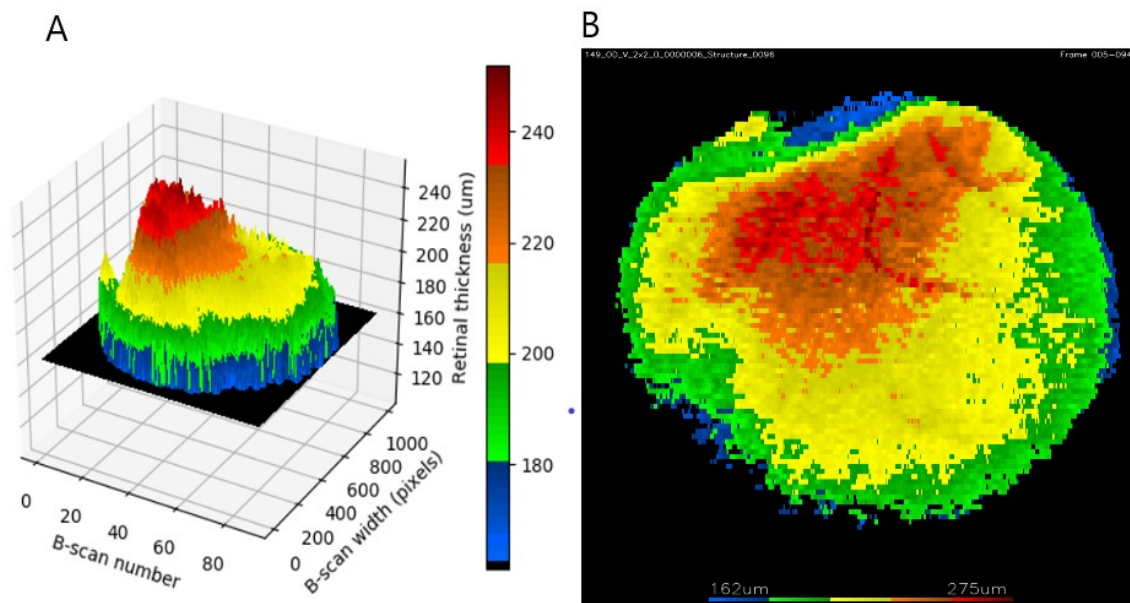
Figure 4.6: **A representative 3D heat map displaying the relative thickness of the whole retina from a complete SD-OCT scan of a 100 dph juvenile cultured lumpfish (a) compared to its 2D representation showed in (b).**
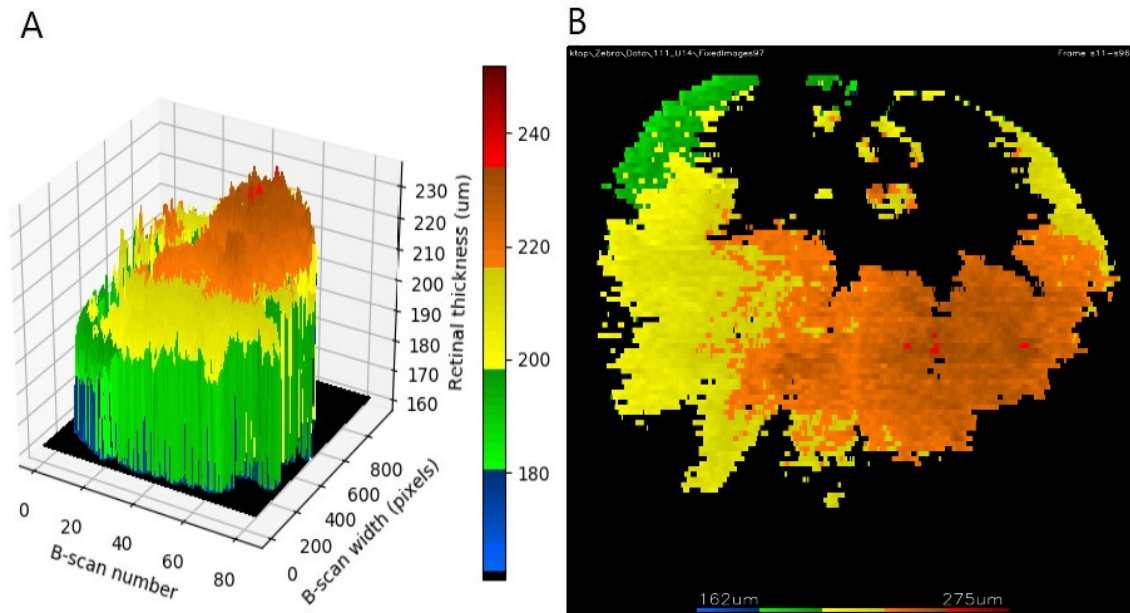
Figure 4.7: **Representative 3D heat map displaying the relative thickness of the whole retina from a zebrafish (a) compared to its 2D representation showed in (b).**

The "en face" view of the image shown in Fig. 4.5 was enhanced with the use of a 3D heatmap to replicate the results of the 2D heatmap (Fig. 4.6), with the before mentioned zebrafish data being shown similarly in (Fig. 4.7). This additional visualization tool gives the user a new perspective on the surface of the retina and a better interpretation of the 3D volume of the SD-OCT retinal scan. The 3D heatmap is particularly useful for both its ability to display the optic nerve as shown in the 2D heatmap and confirmed through analysis of the individual b-scans as seen in (Fig. 4.2 and 4.3) and to represent the relative thickness of the retina. The heatmaps featured in this program are also available according to the viridis colour schemes [57] via a selectable option Fig. 4.8.
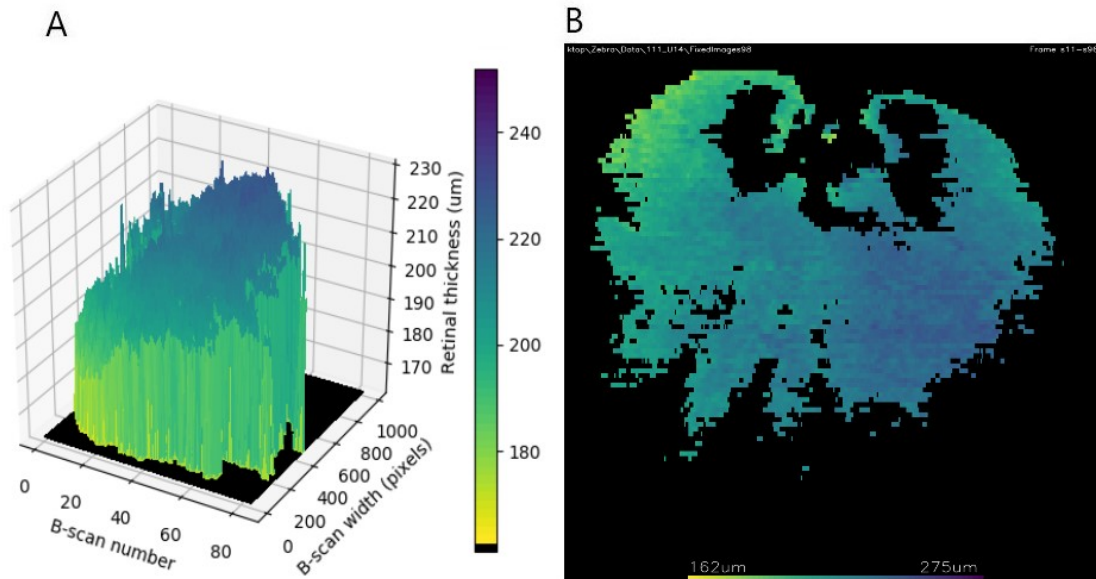
Figure 4.8: **Representative viridis 3D heat map displaying the relative thickness of the whole retina from a zebrafish (a) compared to its 2D representation showed in (b).**

4.1 Human Retina Test

My goal in producing this algorithm was to analyse species analogous to the human retina to give scientists studying the retina a better tool to conduct their research. We have currently seen the application of the algorithm to the task of non-mammalian teleost species. In this section, I will be describing how I tested the algorithm on sources of human retina to test the direct application on both mammalian species and to demonstrate the potential of its future development. The dataset that I used for this human segmentation test was generated by the University of Waterloo's Theoretical and Experimental Epistemology Lab (TEEL) [53]. I have compared the results of this test to the results of our previous retinal segmentation as seen in (Fig.
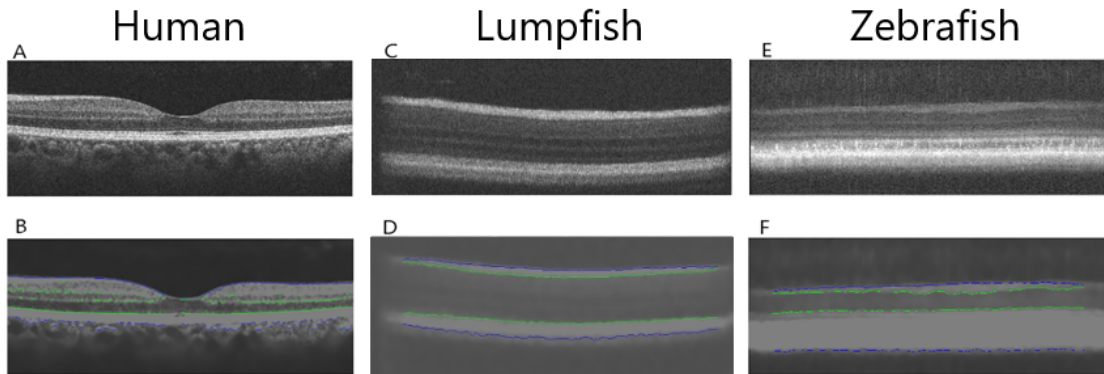
Figure 4.9: **Representative retinal layer identification of both the human (Image 102 [53]), cultured lumpfish and zebrafish.** Consisting of a representative SD-OCT retinal B-scan analysis of each species followed by their analysis using the algorithm with the respective retinal layers identified. Human: original: (a), segmented: (b). Lumpfish original: (c), segmented: (d). Zebrafish original: (e), segmented: (f).

4.9). In this case the algorithm was capable of properly segmenting the NFL/GCL but was not capable of differentiating the choroid layer from the RPE thus could not perform a complete segmentation.

4.2 Discussion

The algorithm has proven robustness in segmenting different retinal features and in its ability to properly delineate the fovea which is a unique feature of human retinal segmentation when compared to the previous species. While it was capable of properly identifying the NFC-GLC region similar to the other species, the OS-RPE layer and the presence of inter-layer blood vessels proved to be more difficult. This

shows that the algorithm is capable of partially completing a human segmentation but would need to be updated in order to fully complete this task. A potential method of solving this problem would be the use of multiple types of algorithms in a combined hybrid solution.

4.3   Future Development

A potential future retinal segmentation algorithm could use a graph theory or machine learning based segmentation method in a combination with novel thresholding to differentiate the RPE from the choroid in (Fig. 4.9). This solution could be then combined with our heat-mapping software to provide a better human SD-OCT assessment tool.

Chapter 5

Conclusions

Our analyses demonstrate that the algorithm can correctly process lumpfish and zebrafish images identifying the thickness of several retinal layers important to the field of vision science. This approach is especially relevant where manual SD-OCT analysis was previously the only method of processing, organising and interpreting SD-OCT data. This program will allow researchers to rapidly and accurately maximize data interpretation in SD-OCT analyses of the retina for a number of teleosts including lumpfish and zebrafish. This obtained data is then combined with a 2D and 3D heatmap program that provides scientists with a new prospective of the whole retinal surface which would be far more difficult through manual measurements alone. The creation of this tool will allow for new knowledge on the physiological systems of both the lumpfish and the zebrafish which is important for better understanding these species.

In the future, a hybrid solution featuring the core technology of this algorithm along with potential additions based on graph-theory and machine learning segmentation could be used to better understand and interpret even more retinal architecture. With this system, clinicians would have the opportunity to quickly assess the retinal health of a patient through retinal analysis and to track this over time similar to how x-rays are used today. This future solution could serve as the basis of a diagnostic system in which neurodegenerative diseases (Doustar et al., 2017 [13]) can be properly accessed and monitored. This solution would be more cost effective and applicable than traditional solutions which cannot be used at scale due to the resource intensive nature of these methods. As this is the case, the potential of a solution that combines research, technology and newly created algorithms has the opportunity to advance the field of medicine in the future.

Chapter 6

Appendix

6.1 Representative data table of a cultured lump-fish segmentation output

B-scan Number	Retinal Thickness (um)	Number of Readings	NFL/GLC (um)	Number of Readings	IPL/INL/OPL/ONL/IS (um)	Number of Readings	OS/RPE (um)	Number of Readings
005	147.6	37	10.6	34	85.9	37	51.8	37
006	168.9	125	26	121	103.3	125	40.4	125
007	181.8	199	31.4	195	108.3	199	42.7	199
008	188.5	260	41.2	254	105.9	260	42.4	259
009	192	357	42	348	109.6	357	41.5	356
010	197.5	381	46.5	371	111.1	381	41.2	380
011	199.2	457	42.3	454	114.7	457	42.5	457
012	201.8	486	44.1	483	114.6	486	43.5	485
013	203.2	541	41.3	537	118.6	541	43.6	540
014	204.1	568	40.7	568	122.8	568	40.5	568
015	205.3	606	40.3	605	126	606	39.1	605
016	207.5	629	42.1	628	128.4	629	37.2	628
017	208.2	645	44	645	130.4	645	33.9	645
018	209.3	667	45.3	664	132	667	32.2	666
019	211.1	697	45.5	696	133.5	697	32.3	692
020	212.7	708	46.2	707	133.8	708	32.9	707
021	215	722	47.7	721	133.2	722	34.2	722
022	215.8	737	49.3	737	132.1	737	34.7	731
023	217.1	753	49.4	752	132.3	753	35.6	752
024	217.9	761	47.9	761	132.9	761	37.3	759
025	217.9	787	46.5	786	133.7	787	37.7	787
026	217.1	801	44.8	801	135.1	801	37.3	799
027	218.3	812	44.5	812	135.5	812	38.3	812
028	218.5	826	43.7	825	136.1	826	38.8	825
029	218.8	831	42.4	831	136.5	831	39.9	830
030	218.4	830	41	829	136.8	830	40.6	830
031	216.4	850	38.6	849	137.9	850	40.1	845
032	217.4	847	38.5	845	137.9	847	41	847
033	217.4	853	37.7	851	138	853	41.7	853
034	216.4	857	37.1	855	138.1	857	41.3	857
035	215.4	862	35.9	860	137.9	862	41.6	862
036	215.6	880	35.3	880	138.3	880	42.1	880
037	214.9	888	34.5	888	137.9	888	42.4	887
038	215.4	894	34.6	892	137.6	894	43.3	894
039	214.5	891	34	890	137.4	891	43.2	890
040	213.1	897	33.1	896	137.2	897	42.8	897
041	213.8	892	33.4	891	136	892	44.5	892
042	213.1	893	33.1	892	136	893	44	893
043	214.2	899	33.2	898	135.5	899	45.5	899
044	212.2	899	32.9	898	134.8	899	44.5	899
045	211.7	909	32.2	907	134.7	909	44.9	909
046	211.2	898	31.4	897	133.9	898	46	898
047	209.4	896	31.1	892	133.8	896	44.6	896
048	208.6	886	30.4	882	132.8	886	45.4	886
049	208.2	897	29.6	896	132.3	897	46.3	897
050	209.2	871	30	870	131.2	871	48	871
051	207.1	898	28.7	897	130.8	898	47.6	898
052	206.2	894	28.2	889	130.7	894	47.3	894
053	205.9	882	28	880	129.6	882	48.3	882
054	204.9	883	27.1	881	129.3	883	48.6	883
055	205	882	27	880	128.5	882	49.5	882
056	204.9	880	25.9	879	128.6	880	50.4	880
057	202.9	892	25.5	891	127.7	892	49.8	892
058	203.4	857	25.7	856	126.4	857	51.4	857
059	202.3	873	25.1	868	126.4	873	50.9	873
060	201.3	871	24	861	126.6	871	50.9	871
061	201.8	863	24.1	862	125.8	863	51.9	863
062	202	818	24	804	124.2	818	54.1	818
063	202.5	791	24.6	775	123.3	791	55.1	791
064	202.3	815	24.7	809	123.3	815	54.5	815
065	200.9	795	23.4	793	123.1	795	54.5	795
066	200.5	779	23.2	771	122.3	779	55.3	779
067	201.2	739	24	723	120.9	739	56.8	739
068	201.3	704	24	696	119.6	704	57.9	704
069	200.9	704	25.7	697	117.9	704	57.5	704
070	202.3	657	27	650	116.6	657	58.9	657
071	201	655	24	652	119	655	58.1	655
072	200.3	674	23.9	672	118.9	674	57.6	674
073	199.8	677	23.7	676	118.3	677	57.8	677
074	198.6	642	22.4	635	117.8	642	58.5	642
075	197.7	577	22.4	563	117.1	577	58.7	577
076	197.4	574	20.1	566	119.1	574	58.4	574
077	196	605	19.6	598	118.5	605	58.2	605
078	197.9	506	20.9	493	116.9	506	60.5	506
079	196	506	20.2	503	116.7	506	59.2	506
080	195.1	477	20.4	462	115.8	477	59.4	477
081	195.8	437	19.6	429	116.9	437	59.6	437
082	194.6	457	20.3	452	116.4	457	58.1	457
083	192.2	437	17.7	424	118.1	437	56.9	437
084	191.7	400	17.9	397	117.1	400	56.8	400
085	189.1	323	14.8	315	118.4	323	56.2	323
086	187.9	272	13.4	264	119.8	272	55	272
087	184.3	171	11.2	155	119.5	171	54.5	171
088	182.4	200	11.3	185	120.6	200	51.2	200
089	181.7	120	8.5	100	120	120	54.2	120
090	173.3	21	4.9	10	127.4	21	42.2	21
091	173.9	8	4.9	4	128.8	8	41.3	8
092	0	0	0	0	0	0	0	0
093	0	0	0	0	0	0	0	0
094	0	0	0	0	0	0	0	0

Specimen: $149ODV2x200000006$; NFL/GCL volume percentage: 14.9; Inner and Outer layers/IS volume percentage: 61.9; OS/RPE: 23.2 volume percentage; Settings: White threshold: 102; Minimum gap threshold: -35; Maximum gap threshold: -135; Minimum thickness: 3. Starting Height: 250; Ending Height: 500; Starting Width: 0; Ending Width: 1000.

6.2   Installation Manual

Required Hardware Any 64-bit Modern operating system including Windows, MacOS, Linux.

Required Software:

1. Python 3.6.3

2. matplotlib 3.1.0

3. numpy 1.17.0

4. opencv-python 3.4.4.19

5. Pillow 6.1.0

6. XlsxWriter 1.1.8

7. xlwt 1.3.0

8. wxPython 4.0.7.post2

Setup: Install all required software and place the files in a directory which containing both a "Data" and an "Images" folder with the included settings.txt file for manual use without the user interface. A requirements file has been included which can be used to install all required software using the "pip install -r requirements.txt" command in the terminal. The requirement file is used with pip, which is a terminal application to install dependencies for the program. The program is then run from the terminal using the command "python ImagePoints-Based.py." The terminal command "pip install -r requirements.txt" while you are in the same directory as the requirements file would then install all the required software. If you have both python 2 and 3 installed, you will need to use the command pip3 and python3 instead of pip and python in the following commands.

1. Navigate to the program directory (folder location) in the terminal

2. run the command "pip install -r requirements.txt"

3. run the command "python ImagePointsBased.py"

For example, if the folder is on your desktop you would have to run the following commands in the terminal:

1. cd Desktop/Foldername

2. pip install -r requirements.txt or For Mac: pip install -U requirements.txt

3. python ImagePointsBased.py

6.3 User Manual

Operation with user interface Open up the program by selecting the "Program.py" file a shortcut to this file can be made and placed on the desktop for better ease of use. The programs user interface will then be presented to the user where the programs settings can be then entered before running the program in a test or full scan mode. The full scan mode will automatically computer the 2D and 3D heatmaps unlike the test mode only processes one image and does not compute

the heatmaps. The images and retuned data will be stored in a marked folder in the projects main folder for all generated scans.

Operation with terminal interface

1. Starting image number

2. Ending image number

3. Image set number (starts at zero)

4. White value threshold

5. Minimum gap value (negative)

6. Maximum gap value (negative)

7. Minimum pixel gap value

8. Storage type (1 = xls, 2 = xlsx, 3 = csv)

9. Heatmap setting (A for automatic else provide a number to compare sets of heatmaps)

10. Smoothing line (S = smoothing line, N = turn off smoothing line)

To run the terminal program, place the data folder into the data directory, adjust all necessary setting then call "python ImagePointsBased.py" or "python ZPointsBased.py" in your terminal. When the program has finished running it will automatically save its results, images and heatmap within their respective directories. Images will be saved in the "Images" folder, with the results and heatmap saved in the working directory. Similarly, when the smoothing line feature is activated, it will save the images in the "SmoothingLine" folder.

Bibliography

[1] Kent R Barter, Hélène Paradis, Robert L Gendron, Josué A Lily Vidal, and Oscar Meruvia-Pastor. Novel segmentation algorithm for high-throughput analysis of spectral domain-optical coherence tomography imaging of teleost retinas. 2022.

[2] Andrew R Whatham, Vincent Nguyen, Yuan Zhu, Michael Hennessy, and Michael Kalloniatis. The value of clinical electrophysiology in the assessment of the eye and visual system in the era of advanced imaging. *Clinical and Experimental Optometry*, 97(2):99–115, 2014.

[3] Lindsey L Glickfeld, R Clay Reid, and Mark L Andermann. A mouse model of higher visual cortical function. *Current opinion in neurobiology*, 24:28–33, 2014.

[4] Giuseppe Bianco, Robin Clemens Köhler, Mihaela Ilieva, and Susanne Åkesson. Magnetic body alignment in migratory songbirds: a computer vision approach. *Journal of Experimental Biology*, 222(5), 2019.

[5] Chantal Dysli, Volker Enzmann, Raphael Sznitman, and Martin S Zinkernagel. Quantitative analysis of mouse retinal layers using automated segmentation of spectral domain optical coherence tomography images. *Translational vision science & technology*, 4(4):9–9, 2015.

[6] Pratul P Srinivasan, Stephanie J Heflin, Joseph A Izatt, Vadim Y Arshavsky, and Sina Farsiu. Automatic segmentation of up to ten layer boundaries in sd-oct images of the mouse retina with and without missing layers due to pathology. *Biomedical optics express*, 5(2):348–365, 2014.

[7] Brent A Bell, Alex Yuan, Rose M Dicicco, Joseph Fogerty, Emma M Lessieur, and Brian D Perkins. The adult zebrafish retina: in vivo optical sectioning with confocal scanning laser oph-

thalmoscopy and spectral-domain optical coherence tomography. *Experimental eye research*, 153:65–78, 2016.

[8] Raahyma Ahmad, Helene Paradis, Danny Boyce, James McDonald, and Robert L Gendron. Novel characteristics of the cultured lumpfish cyclopterus lumpus eye during post-hatch larval and juvenile developmental stages. *Journal of fish biology*, 94(2):297–312, 2019.

[9] Shibin Wu, Shaode Yu, Ling Zhuang, Xinhua Wei, Mark Sak, Neb Duric, Jiani Hu, and Yaoqin Xie. Automatic segmentation of ultrasound tomography image. *BioMed research international*, 2017, 2017.

[10] Rachel Linderman, Alexander E Salmon, Margaret Strampe, Madia Russillo, Jamil Khan, and Joseph Carroll. Assessing the accuracy of foveal avascular zone measurements using optical coherence tomography angiography: segmentation and scaling. *Translational vision science & technology*, 6(3):16–16, 2017.

[11] Maria Toms, Dhani Tracey-White, Dhakshi Muhundhakumar, Lina Sprogyte, Adam M Dubis, and Mariya Moosajee. Spectral domain optical coherence tomography: an in vivo imaging protocol for assessing retinal morphology in adult zebrafish. *Zebrafish*, 14(2):118–125, 2017.

[12] Preeti Patil Chhablani, Vikas Ambiya, Akshay G Nair, Sailaja Bondalapati, and Jay Chhablani. Retinal findings on oct in systemic conditions. In *Seminars in Ophthalmology*, volume 33, pages 525–546. Taylor & Francis, 2018.

[13] Jonah Doustar, Tania Torbati, Keith L Black, Yosef Koronyo, and Maya Koronyo-Hamaoui. Optical coherence tomography in alzheimer's disease and other neurodegenerative diseases. *Frontiers in neurology*, 8:701, 2017.

[14] Laurel N Vuong and Thomas R Hedges. Ganglion cell layer complex measurements in compressive optic neuropathy. *Current Opinion in Ophthalmology*, 28(6):573–578, 2017.

[15] M Bolton-Warberg. An overview of cleaner fish use in ireland. *Journal of fish diseases*, 41(6):935–939, 2018.

[16] Adam J Brooker, Athina Papadopoulou, Carolina Gutierrez, Sonia Rey, Andrew Davie, and Herve Migaud. Sustainable production and use of cleaner fish for the biological control of sea lice: recent advances and current challenges. *Veterinary Record*, 183(12):383–383, 2018.

[17] Adam Powell, Jim W Treasurer, Craig L Pooley, Alex J Keay, Richard Lloyd, Albert K Imsland, and Carlos Garcia de Leaniz. Use of lumpfish for sea-lice control in salmon farming: challenges and opportunities. *Reviews in Aquaculture*, 10(3):683–702, 2018.

[18] P Lorance, R Cook, J Herrera, L de Sola, A Florin, and C Papaconstantinou. Cyclopterus lumpus. *The IUCN Red List of Threatened Species*, 2015.

[19] Committee on the Status of Endangered Wildlife in Canada (COSEWIC), Government of Canada., 1977.

[20] Helene Paradis, Raahyma Ahmad, James McDonald, Danny Boyce, and Robert L Gendron. Ocular tissue changes associated with anterior segment opacity in lumpfish (cyclopterus lumpus l) eye. *Journal of fish diseases*, 42(10):1401–1408, 2019.

[21] Laia Ribas and Francesc Piferrer. The zebrafish (d anio rerio) as a model organism, with emphasis on applications for finfish aquaculture research. *Reviews in Aquaculture*, 6(4):209–240, 2014.

[22] Ross F Collery, Kerry N Veth, Adam M Dubis, Joseph Carroll, and Brian A Link. Rapid, accurate, and non-invasive measurement of zebrafish axial length and other eye dimensions using sd-oct allows longitudinal analysis of myopia and emmetropization. *PLoS One*, 9(10):e110699, 2014.

[23] Jing Tian, Boglárka Varga, Gábor Márk Somfai, Wen-Hsiang Lee, William E Smiddy, and Delia Cabrera DeBuc. Real-time automatic segmentation of optical coherence tomography volume data of the macular region. *PloS one*, 10(8):e0133908, 2015.

[24] Wolf M. Harmening and Lawrence C. Sincich. Adaptive optics for photoreceptor-targeted psychophysics. *High Resolution Imaging in Microscopy and Ophthalmology, Fig. 17.1*, page 359–375, 2019.

[25] Nicola K Cassels, John M Wild, Tom H Margrain, Victor Chong, and Jennifer H Acton. The use of microperimetry in assessing visual function in age-related macular degeneration. *Survey of ophthalmology*, 63(1):40–55, 2018.

[26] Fiona Costello and Jodie M Burton. Retinal imaging with optical coherence tomography: a biomarker in multiple sclerosis? *Eye and brain*, 10:47, 2018.

[27] Yoo-Ri Chung, Young Ho Kim, Seong Jung Ha, Hye-Eun Byeon, Chung-Hyun Cho, Jeong Hun Kim, and Kihwang Lee. Role of inflammation in classification of diabetic macular edema by optical coherence tomography. *Journal of Diabetes Research*, 2019, 2019.

[28] Lele Huang, Chen Wang, Wanting Wang, Yujie Wang, and Ruijun Zhang. The specific pattern of retinal nerve fiber layer thinning in

parkinson's disease: a systematic review and meta-analysis. *Journal of Neurology*, 268(11):4023–4032, 2021.

[29] Ethan Waisberg and Jonathan A Micieli. Neuro-ophthalmological optic nerve cupping: An overview. *Eye and Brain*, 13:255, 2021.

[30] Jee-Young Lee, Antonio Martin-Bastida, Ane Murueta-Goyena, Iñigo Gabilondo, Nicolás Cuenca, Paola Piccini, and Beomseok Jeon. Multimodal brain and retinal imaging of dopaminergic degeneration in parkinson disease. *Nature Reviews Neurology*, 18(4):203–220, 2022.

[31] Akshaya Mishra, Alexander Wong, Kostadinka Bizheva, and David A Clausi. Intra-retinal layer segmentation in optical coherence tomography images. *Optics express*, 17(26):23719–23728, 2009.

[32] Azadeh Yazdanpanah, Ghassan Hamarneh, Benjamin Smith, and Marinko Sarunic. Intra-retinal layer segmentation in optical coherence tomography using an active contour approach. In *Inter-*

national Conference on Medical Image Computing and Computer-Assisted Intervention, pages 649–656. Springer, 2009.

[33] Qi Yang, Charles A Reisman, Zhenguo Wang, Yasufumi Fukuma, Masanori Hangai, Nagahisa Yoshimura, Atsuo Tomidokoro, Makoto Araie, Ali S Raza, Donald C Hood, et al. Automated layer segmentation of macular oct images using dual-scale gradient information. *Optics express*, 18(20):21293–21307, 2010.

[34] Olaf Ronneberger, Philipp Fischer, and Thomas Brox. U-net: Convolutional networks for biomedical image segmentation. In *International Conference on Medical image computing and computer-assisted intervention*, pages 234–241. Springer, 2015.

[35] Leyuan Fang, David Cunefare, Chong Wang, Robyn H Guymer, Shutao Li, and Sina Farsiu. Automatic segmentation of nine retinal layer boundaries in oct images of non-exudative amd patients using deep learning and graph search. *Biomedical optics express*, 8(5):2732–2744, 2017.

[36] Ferozuddin Riaz and Khidir M Ali. Applications of graph theory in computer science. In *2011 Third International Conference on Computational Intelligence, Communication Systems and Networks*, pages 142–145. IEEE, 2011.

[37] Pascal A Dufour, Lala Ceklic, Hannan Abdillahi, Simon Schroder, Sandro De Dzanet, Ute Wolf-Schnurrbusch, and Jens Kowal. Graph-based multi-surface segmentation of oct data using trained hard and soft constraints. *IEEE transactions on medical imaging*, 32(3):531–543, 2012.

[38] Mona K Garvin, Michael D Abràmoff, Randy Kardon, Stephen R Russell, Xiaodong Wu, and Milan Sonka. Intraretinal layer segmentation of macular optical coherence tomography images using optimal 3-d graph search. *IEEE transactions on medical imaging*, 27(10):1495–1505, 2008.

[39] Wenjun Duan, Yuanjie Zheng, Yanhui Ding, Sujuan Hou, Yufang Tang, Yan Xu, Maoling Qin, Jianfeng Wu, Dinggang Shen, and Hongsheng Bi. A generative model for oct retinal layer segmenta-

tion by groupwise curve alignment. *IEEE Access*, 6:25130–25141, 2018.

[40] Loza Bekalo, Sijie Niu, Xiaojun He, Ping Li, Idowu Paul Okuwobi, Chenchen Yu, Wen Fan, Songtao Yuan, and Qiang Chen. Automated 3-d retinal layer segmentation from sd-oct images with neurosensory retinal detachment. *IEEE Access*, 7:14894–14907, 2019.

[41] Shiliang Lou, Xiaodong Chen, Xiaoyan Han, Jing Liu, Yi Wang, and Huaiyu Cai. Fast retinal segmentation based on the wave algorithm. *IEEE Access*, 8:53678–53686, 2020.

[42] Yushu Ma, Yingzhe Gao, Zhaolin Li, Ang Li, Yi Wang, Jian Liu, Yao Yu, Wenbo Shi, and Zhenhe Ma. Automated retinal layer segmentation on optical coherence tomography image by combination of structure interpolation and lateral mean filtering. *Journal of Innovative Optical Health Sciences*, 14(01):2140011, 2021.

[43] Andrew Lang, Aaron Carass, Matthew Hauser, Elias S Sotirchos,

Peter A Calabresi, Howard S Ying, and Jerry L Prince. Retinal layer segmentation of macular oct images using boundary classification. *Biomedical optics express*, 4(7):1133–1152, 2013.

[44] Abhijit Guha Roy, Sailesh Conjeti, Sri Phani Krishna Karri, Debdoot Sheet, Amin Katouzian, Christian Wachinger, and Nassir Navab. Relaynet: retinal layer and fluid segmentation of macular optical coherence tomography using fully convolutional networks. *Biomedical optics express*, 8(8):3627–3642, 2017.

[45] Alessio Montuoro, Sebastian M Waldstein, Bianca S Gerendas, Ursula Schmidt-Erfurth, and Hrvoje Bogunović. Joint retinal layer and fluid segmentation in oct scans of eyes with severe macular edema using unsupervised representation and auto-context. *Biomedical optics express*, 8(3):1874–1888, 2017.

[46] Chuang Wang, Ya Xing Wang, and Yongmin Li. Automatic choroidal layer segmentation using markov random field and level set method. *IEEE journal of biomedical and health informatics*, 21(6):1694–1702, 2017.

[47] Abhay Shah, Leixin Zhou, Michael D Abrámoff, and Xiaodong Wu. Multiple surface segmentation using convolution neural nets: application to retinal layer segmentation in oct images. *Biomedical optics express*, 9(9):4509–4526, 2018.

[48] Qi Song, Junjie Bai, Mona K Garvin, Milan Sonka, John M Buatti, and Xiaodong Wu. Optimal multiple surface segmentation with shape and context priors. *IEEE transactions on medical imaging*, 32(2):376–386, 2012.

[49] Svetlana Borkovkina, Acner Camino, Worawee Janpongsri, Marinko V Sarunic, and Yifan Jian. Real-time retinal layer segmentation of oct volumes with gpu accelerated inferencing using a compressed, low-latency neural network. *Biomedical Optics Express*, 11(7):3968–3984, 2020.

[50] Ai Ping Yow, Bingyao Tan, Jacqueline Chua, Tin Aung, Rahat Husain, Leopold Schmetterer, and Damon Wong. Automated circumpapillary retinal nerve fiber layer segmentation in high-resolution swept-source oct. In *2020 42nd Annual International Conference*

of the IEEE Engineering in Medicine & Biology Society (EMBC), pages 1832–1835. IEEE, 2020.

[51] Daniel E O'Leary. Artificial intelligence and big data. *IEEE intelligent systems*, 28(2):96–99, 2013.

[52] Ryan T Yanagihara, Cecilia S Lee, Daniel Shu Wei Ting, and Aaron Y Lee. Methodological challenges of deep learning in optical coherence tomography for retinal diseases: a review. *Translational Vision Science & Technology*, 9(2):11–11, 2020.

[53] Peyman Gholami, Priyanka Roy, Mohana Kuppuswamy Parthasarathy, and Vasudevan Lakshminarayanan. Octid: Optical coherence tomography image database. *Computers & Electrical Engineering*, 81:106532, 2020.

[54] Perkin Elmer. Openlab 5.5 developed by perkin elmer, 2010.

[55] Kent Robert Barter. Sd-oct-points-based. `https://github.com/krbarter/SD-OCT-Points-Based`, 2022.

[56] G. Bradski. The OpenCV Library. *Dr. Dobb's Journal of Software Tools*, 2000.

[57] Garnier, Simon, Ross, Noam, Rudis, Robert, Camargo, Antônio Pedro, Sciaini, Marco, Scherer, and Cédric. *viridis - Colorblind-Friendly Color Maps for R*, 2021. R package version 0.6.2.